A YY1 phosphorylation switch in brown adipose tissue orchestrates energy homeostasis.

Zyanya Díaz-Hirashi
University of Zurich
Tian Gao
University of Zurich
Chiara Scaffidi
University of Zurich
Monika Fey
University of Zurich
Susan Murray
Ionis Pharmaceuticals, Carlsbad, California
Audrey Low
Ionis Pharmaceuticals https://orcid.org/0000-0002-9960-9849
Olga Pushkareva
Ecole Polytechnique Fédérale de Lausanne (EPFL)
Raed Rizkallah
College of Medicine, Florida State University
Bart Deplancke
École Polytechnique Fédérale de Lausanne (EPFL) https://orcid.org/0000-0001-9935-843X
Francisco Verdeguer (francisco.verdeguer@dmmd.uzh.ch)
University of Zurich https://orcid.org/0000-0002-5798-1503

Article

Keywords: energy homeostasis, energy balance, brown adipose tissue, YY1 phosphorylation switch

Posted Date: June 12th, 2021

DOI: https://doi.org/10.21203/rs.3.rs-523586/v1

A YY1 phosphorylation switch in brown adipose tissue orchestrates energy homeostasis.

Zyanya Díaz-Hirashi[1], Tian Gao[1], Chiara Scaffidi[1], Monika Fey[1], Sue Murray[2], Audrey Low[2], Olga Pushkareva[3], Raed Rizkallah[4], Bart Deplancke[3] and Francisco Verdeguer[1].

[1] Department of Molecular Mechanisms of Disease, University of Zurich. Switzerland.

[2] Ionis Pharmaceuticals, Carlsbad, California. United States.

[3] Ecole Polytechnique Fédérale de Lausanne (EPFL). Lausanne, Switzerland.

[4] College of Medicine, Florida State University, USA.

ABSTRACT.

Whole-body energy homeostasis is influenced by anabolic and catabolic cellular programs, which depend on environmental and nutritional cues. Adipose tissue plays a predominant role in the physiological regulation of energy balance by either storing or consuming energy through brown adipose tissue thermogenesis. It is however not clearly understood how brown adipose tissue balances catabolic and anabolic states. We show here that the transcription factor YY1 senses energetic state through a post-translational S120 phosphorylation switch. Adrenergic signaling leads to YY1 dephosphorylation which directly activates thermogenesis and a catabolic gene program while its phosphorylation maintains an anabolic program. Mechanistically, YY1 dephosphorylation increases chromatin binding at distal genomic loci respective to the transcription start site but remains constitutively bound to TSS. This mode of transcriptional control influences the activating and repressive function of YY1 and regulates catabolism/anabolism. We show that YY1 interacts with PPP1R3B, a regulatory subunit of the phosphatase PP1 and that *in vivo* knockdown of PPP1R3B protects against diet-induced obesity and insulin resistance. Our results uncover a novel transcriptional mechanism of metabolism orchestrated by YY1 phosphorylation switch and identifies PPP1R3B as a regulator of energy balance.

INTRODUCTION.

The adipose tissue contributes to the regulation of the whole-body energy equilibrium by balancing catabolic versus anabolic functions (Rosen and Spiegelman, 2014). A part of the energy homeostasis is controlled by adaptive thermogenesis in the brown adipose tissue (BAT) (Cohen and Kajimura, 2021). The activation of brown adipose tissue thermogenesis leads to increased metabolic rate and consumption of nutrients, effects that are associated with improved metabolic health (Chouchani et al., 2019). Identifying novel pathways that favor energy expenditure through increased thermogenesis is a current promising therapeutic approach for metabolic disorders (Giordano et al., 2016; Kusminski et al., 2016). The classical mechanism of thermogenesis in brown and inducible beige adipocytes is through the elevation of the uncoupling protein 1 (UCP1). UCP1 dissipates the mitochondrial proton gradient, resulting in an inefficient ATP synthesis which leads to increased catabolism of glucose and fatty acids producing heat loss as a by-product (Cannon and Nedergaard, 2004). Cold exposure triggers a sympathetic adrenergic signaling and several hormonal responses activate the expression of UCP1 in brown and beige adipocytes (Cannon and Nedergaard, 2004; Scheele and Wolfrum, 2020).

Upon obesogenic and high nutrient conditions, brown adipocytes reduce their thermogenic potential and acquire a white phenotype (Bonet et al., 2017; Sanchez-Gurmaches and Guertin, 2014; Shao et al., 2016). This is associated with reduced UCP1 expression and oxidation of nutrients, as well as increased anabolism. At the cellular signaling level, energetic status is sensed by central kinases AMPK and mTOR that signal to downstream effectors to control opposite catabolic and anabolic responses respectively (González et al., 2020; Hardie et al., 2016). Specific transcription factors or co-activators including PPARγ, PGC-1α, FOXO, HNF4α, SREBP or ChREBP sense and/or control nutrient and energetic status in adipose tissue by integrating cell signaling cascades and coordinating a thermogenic and energetic response(Eguchi et al., 2011; Feige and Auwerx, 2007; Lefterova et al., 2014; Puigserver and Spiegelman, 2003; Spiegelman et al., 2009). It is not known how several transcription factors

are hierarchically regulated and interact with general transcription factors and whether robust and redundant transcriptional mechanisms are required to sense and control the balance between catabolic and anabolic decisions.

Yin Yang 1 (YY1) is a ubiquitously expressed transcription factor that orchestrates multiple cellular processes and functions (Gordon et al., 2006). Recently, YY1 has been identified as a structural transcription factor that controls long range DNA interactions (Weintraub et al., 2017). YY1's ubiquitous expression suggests a fundamental role in transcription regulation as well as being a candidate for basal and robust control of transcriptional programs. Previous work showed that YY1 controls whole-body energy balance through brown adipose tissue function (Verdeguer et al., 2016). However, the upstream signals that control YY1 function are unknown. Adrenergic signaling is the canonical activation pathway of adipose tissue thermogenesis. This is mediated through increased cAMP levels followed by the activation of PKA, leading to subsequent phosphorylation events. The role of phosphatases in this pathway remains however unexplored. Adrenergic signaling in brown adipose tissue is the target of current pharmacological strategies (Blondin et al., 2020; Cypess et al., 2015). It is therefore important to understand the regulatory elements and transcriptional downstream effects of this pathway.

We have identified a phosphorylation switch of YY1 in response to adrenergic signaling in adipocytes. We show here that YY1(S120) dephosphorylation leads to increased thermogenesis and favors catabolic versus anabolic responses. We discovered PPP1R3B as a mediator of YY1 phosphorylation and a regulator of whole-body energy homeostasis.

RESULTS.

Adrenergic signaling leads to YY1(S120) dephosphorylation in brown adipose tissue.

Adrenergic signaling is the canonical pathway of thermogenic activation in brown adipocytes. Our previous data showed that YY1 plays a key role in metabolism and energy balance (Verdeguer et al., 2016). The upstream regulators of YY1 remain elusive. We sought here to

investigate how YY1 orchestrates environmental signals. The S120 phosphorylation in mice is a highly conserved and significant site identified by Phosphosite (Figure 1A and Suppl. Fig 1A). It is located in the transactivation domain of YY1 and corresponds to S118 in humans (Hornbeck et al., 2015). Its function is however poorly understood. We have discovered that YY1(S120) phosphorylation status is influenced by different energetic stimuli. We found that 12h of cold exposure in C57BL6/J mice induces a dephosphorylation at S120 of YY1 in brown adipose tissue (Figure 1B and Suppl. Fig. 1B-D), suggesting an interaction between YY1 and adrenergic signaling. To test this hypothesis, we treated brown adipocytes (pBAT) with forskolin (FSK), which mediates an increase in cAMP by the activation of adenylate cyclase, a component of the beta-adrenergic receptor. FSK led to YY1(S120) dephosphorylation in a time-dependent manner compared to vehicle-treated cells (Figure 1C and Suppl. Fig. 1E). Cold exposure triggers a catabolic phenotype. In order to understand the dynamics of YY1 phosphorylation upon an opposite stimulus, we challenged C57BL6/J mice to high fat diet feeding (HFD). In this case, YY1(S120) phosphorylation is increased in BAT and inguinal subcutaneous white adipose tissue (IWAT) (Figure 1D-E). These results show that YY1 is influenced by nutritional and energetic state through its S120 phosphorylation, and this could modulate downstream metabolic effects.

YY1(S120) dephosphorylation in brown adipocytes induces thermogenesis.

In order to understand whether YY1 phosphorylation status orchestrates a metabolic program downstream of adrenergic signaling, we generated the amino acid substitutions S120A and S120E to either abrogate or mimic YY1 phosphorylation respectively. Brown adipocytes (De23) stably expressing GFP, Flag-YY1, Flag-YY1(S120A) or Flag-YY1(S120E) were generated by lentiviral infection followed by puromycin selection and all cell lines reached terminal differentiation (Suppl. Fig. 1F). The generated brown adipocytes overexpress Flag-YY1 wildtype and point mutations over GFP control (Figure 1F) at the mRNA level. Although YY1 is still endogenously expressed, Flag-YY1 wildtype and mutants are expressed at similar

amounts to the endogenous levels measured by WB (Figure 1F and Suppl. Fig. 1G). Our results show that brown adipocytes expressing Flag-YY1(S120A) led to an induction of UCP1 expression at both protein and mRNA levels compared to GFP or Flag-YY1 control (Figure 1F, G). The increase in UCP1 levels was in addition, accompanied by the elevation of other thermogenic and mitochondrial markers including *Pgc1a*, *Cox7a1* and *Cyc1* (Figure 1G). On the other hand, the expression of the phospho-mimetic Flag-YY1(S120E) did not induce UCP1 overexpression or other thermogenic/mitochondrial markers that were induced upon Flag-YY1(S120A) overexpression (Figure 1F, G). Brown adipocytes overexpressing Flag-YY1(S120A) still have endogenous levels of YY1 which are presumably phosphorylated. Nevertheless, YY1(S120A) expression was sufficient to induce the expression of UCP1. In order to challenge this experiment, we treated our generated YY1-mutant brown adipocyte cell lines with FSK to pharmacologically induce endogenous YY1 dephosphorylation. In this experiment, YY1 dephosphorylation would occur on its endogenous levels but would not affect the YY1(S120) point mutations (Suppl. Fig. 1H). First, untreated YY1(S120A) cells displayed UCP1 induction which was not observed withYY1(S120E), further recapitulating our findings (Suppl. Fig. 1H). Upon FSK treatment, there was no induction of UCP1 in the Flag-YY1(S120E) compared to Flag-YY1(S120A) (Suppl. Fig. 1H), confirming that the overexpressed YY1 mutants override the endogenous YY1 effects.

Altogether, these results suggest that YY1 dephosphorylation at S120 triggers a thermogenic response. In order to confirm this hypothesis, we performed oxygen consumption experiments to assess the effect of YY1(S120) dephosphorylation. Brown adipocytes expressing YY1(S120A) showed a significant elevation of oxygen consumption rate measured by Seahorse© technology at basal state (Figure 1H).

Transcriptional role of YY1(S120) phosphorylation in anabolic and catabolic responses.

Our results show that YY1(S120) dephosphorylation activates thermogenesis in brown adipocytes. In order to investigate how YY1 phosphorylation status controls the

transcriptional program of brown adipocytes we performed RNAseq of YY1 wildtype versus YY1(S120A) mutant brown adipocytes. The results show that YY1(S120) dephosphorylation elicits a profound transcriptional reprogramming with more than 269 genes being more than 2-fold up- or down-regulated (Figure 2A). Biological pathway analysis using KEGG enrichment, showed that upregulated thermogenic genes are overrepresented (Figure 1B-C). In addition, Gene Set Enrichment Analysis (GSEA) (Mootha et al., 2003; Subramanian et al., 2005) shows that several catabolic pathways including TCA cycle, fatty acid degradation, glycolysis or oxidative phosphorylation are elevated (Figure 2D). On the contrary, anabolic pathways like mTOR signaling, basal transcription factor or ribosome biogenesis are downregulated. These data are in agreement with the thermogenic phenotype of YY1(S120) dephosphorylation. Altogether, these results suggest that YY1(S120) phosphorylation plays a switching role between catabolic and anabolic processes. To address this hypothesis, we looked at how YY1 phosphorylation status affects the canonical signaling regulators of metabolism AMPK and mTOR. Activation of AMPK by Thr172 phosphorylation (pAMPK(Thr172) enhances catabolism for ATP production. Our results showed that YY1(S120A) cells have increased pAMPK(Thr172) consistent with the increased catabolic phenotype of brown adipocytes upon YY1(S120) dephosphorylation (Figure 2E). The central sensor of nutrient status, mammalian target of Rapamycin (mTOR) and one of its downstream targets, Ribosomal protein S6 kinase beta-1 (p70S6K), were strongly phosphorylated upon YY1(S120) dephosphorylation (Figure 2E). Our hypothesis is that YY1(S120) dephosphorylation activates catabolism. Here, mTOR and S70S6K, that control cell growth and anabolism are hyperactivated upon S120 dephosphorylation, leading to a paradoxical result. This could be explained by a compensatory signaling of the mTOR and p70S6K pathways which have reduced expression of their downstream effectors caused by YY1(S120) dephosphorylation. Our findings are consistent with previous studies showing a loss of YY1 function where pMTOR and p70S6K are hyperactivated (Blättler et al., 2012).

Genome-wide role of YY1 phosphorylation in the control of metabolism.

To understand the genome-wide role of YY1 phosphorylation, we performed global ChIP-seq profiling of brown adipocytes stimulated with FSK or DMSO control to induce a YY1(S120) dephosphorylated and phosphorylated state respectively. As expected, promoters were the most frequent genomic feature (~60%) bound by YY1 in both control and FSK condition (Figure 3A, B). In addition, the unbiased search of DNA motifs under enriched peaks showed the consensus YY1 binding site as the first hit (Figure 3B). Pathway enrichment analysis of the identified YY1 binding sites using ChIPseeqer and clusterProfiler (Giannopoulou and Elemento, 2011) revealed thermogenesis and ribosome among the significantly enriched pathways (Figure 3C). In order to understand how YY1 regulates thermogenesis, we asked how YY1 phosphorylation status could affect *Ucp1* expression. We hypothesized that S120 phosphorylation could affect YY1 recruitment at the *Ucp1* locus. The ChIPseq data at the *Ucp1* enhancer/promoter regions showed an increased YY1 enrichment in its unphosphorylated state upon FSK stimulation compared to control (Figure 3D). We confirmed the increase of the FSK-dependent YY1 enrichment by ChIP-qPCR at -4.9 Kb and -6 Kb loci upstream of *Ucp1* TSS (Figure 3E). To corroborate that the differential binding depends on the YY1(S120) phosphorylation status, we performed a ChIP-qPCR using YY1(pS120) antibodies upon FSK or DMSO control. Here, the phosphorylated YY1 binding at -6 Kb of *Ucp1* TSS was not detected in either control or FSK, suggesting that only unphosphorylated YY1 binds this locus (Figure 3F). In addition, the detected binding of YY1 at -4.9 Kb was reduced upon FSK stimulation confirming that phosphorylated YY1 has a reduced recruitment to this locus (Figure 3E). To further confirm whether YY1 phosphorylation controls *Ucp1* expression through its differential binding to the *Ucp1* enhancer, we performed a luciferase reporter assay using an enhancer sequence of *Ucp1* (Abe et al., 2015). Our data showed that YY1(S120A) construct leads to higher luciferase reporter expression than YY1 wildtype (Figure 3G). Collectively, these results suggest that YY1 phosphorylation status directly controls the transcription of *Ucp1*.

To identify and understand how YY1 phosphorylation status controls the expression of its direct targets, we integrated our RNAseq data of YY1 wildtype and YY1(S120A) with our ChIPseq data of brown adipocytes. We plotted YY1 ChIPseq enrichment (CTR and FSK) over the 10 Kb spanning the TSS of differentially regulated genes of YY1(S120A) versus wildtype (Figure 3H-I). We identified 2 clusters of genes (C1 and C2, Figure 3H-I) in each respective group of down- and upregulated genes where YY1 is bound in the CTR condition, suggesting a direct transcriptional control of these genes (Figure 3H-I). Interestingly, FSK, that elicits YY1(S120) dephosphorylation, did not affect the binding of YY1 on the TSS of these genes. The GO Enrichment Analysis (Mi et al., 2013) of these genes showed an overrepresentation of ribosomal and translation genes in the group of downregulated targets (Data not shown). This suggests that YY1(S120) dephosphorylation plays a suppressor role of ribosomal and translation genes while being retained at the respective TSS. Upregulated genes showed a similar patter, where FSK did not elicit changes in YY1 binding at the TSS (Figure 3I), however these genes were not overrepresented in any functional classification.

We then asked whether FSK induces YY1 binding changes across the whole genome. For that we looked for differential binding using HOMER and showed that YY1 was differentially recruited at 227 loci (Figure 4A). Our data demonstrate that the FSK mediated YY1(S120) dephosphorylation elicits a gain of binding at loci but not loss of binding (Figure 4A). The MEME analysis of the consensus DNA motifs of these binding sites showed a slight modification of the global YY1 consensus binding site (Figure 4B). The genomic analysis of these regulated loci showed that they are located distantly respective of the nearest gene TSS (Figure 4B). Among these genes, our analysis revealed a gain of YY1 binding upon FSK stimulation at 2 interesting loci of genes encoding the Protein Kinase CAMP-Dependent Type II Regulatory Subunit Beta (*Prkar2b*) and Adenylate Cyclase 3 (*Adcy3)*. Both *Prkar2b* and *Adcy3* are essential elements of the adrenergic signaling cascade which are highly selectively expressed in brown adipose tissue (Suppl. Fig. 2A, B). The binding of YY1 is located at -39 Kb and +19 Kb of the TSS of *Prkar2b* and *Adcy3* respectively and we speculated that these

loci could control the transcription of these genes (Figure 4C and Suppl. Fig. 2C). Interestingly, YY1(S120A) leads to the increased expression of *Prkar2b* (Figure 4D). Although YY1(S120A) did not induce *Adcy3* expression, it was highly upregulated in brown adipose tissue of cold-exposed mice (Suppl. Fig. 2D). We then analyzed published Hi-C data of adipocytes (Siersbæk et al., 2017) and showed that these distant YY1 binding sites in the *Prkar2b* and *Adcy3* loci significantly interact with the respective TSS regions, suggesting the existence of a regulatory chromatin loop (Figure 4E and Suppl. Fig. 4E).

CK2 phosphorylates YY1 at S120 in brown adipocytes.

To identify upstream regulators of YY1 phosphorylation status, we first searched for potential conserved kinases motifs surrounding S120. YY1 is conserved across multiple species and S120 is maintained across vertebrate species (Suppl. Fig. 3A). The S120 coincides with a consensus site for Casein Kinase 2 (CK2) identified by Scansite 4.0 (Obenauer et al., 2003) (Suppl. Fig. 3B). Previous work has found CK2 as a direct kinase of YY1(S120) phosphorylation (Riman et al., 2012). Consistent with this published work, our data show that CK2 phosphorylates YY1 in a cold and hot kinase assay (Figure 5A, and Suppl. Fig. 3C-D). In Suppl. Fig. 3C, Flag-YY1 or Flag-YY1(S120A) was purified from transfected U2OS cells using anti-Flag antibodies. YY1 phosphorylation was then detected using YY1(pS120) antibodies. Although YY1 is already endogenously phosphorylated from the U2OS cell extracts, we showed that it is further phosphorylated when incubated with recombinant CK2 in vitro (Figure 4B). Then, the same experiment was performed from GST-purified YY1 expressed in *E. coli* which lacks any basal YY1(S120) phosphorylation. In this case, the phosphorylation of YY1 is only observed upon recombinant CK2 incubation *in vitro*, detected by WB using anti-YY1(pS120) (Figure 5A). Similarly, a hot kinase assay with the incubation of CK2 and YY1 using ^{32}P-labeled ATP showed that YY1 is phosphorylated by CK2 at S120 (Suppl. Fig. 3D-E). In order to investigate if CK2 phosphorylates YY1 also in brown adipocytes, we treated pBAT cells with a CK2 inhibitor; 4,5,6,7-tetrabromobenzotriazole (TBB) or FSK as control. Our WB experiments showed that CK2 inhibition reduces YY1(S120) phosphorylation similarly to

FSK induction (Figure 5B). These data suggest that CK2 is a regulator of YY1 phosphorylation status in brown adipocytes.

Our results have shown that YY1 dephosphorylation increases thermogenesis of brown adipocytes. Since YY1 is phosphorylated by CK2 and YY1 dephosphorylation leads to increased thermogenesis, CK2 inhibition would potentially lead to increased thermogenesis. A previous report of a kinase screen and adipocyte thermogenic function has interestingly identified CK2 as a negative regulator of thermogenesis (Shinoda et al., 2015). In agreement with these findings, our results show that blocking CK2 with TBB, leads to increased UCP1 expression in brown adipocytes (Figure 5B).

Identification of PPP13RB as a regulator of YY1 phosphorylation.

CK2 is a ubiquitously expressed kinase that targets multiple effectors. We hypothesize that additional regulators including phosphatases or regulatory subunits of phosphatases may control YY1 phosphorylation status. To answer this question, we mined proteomic datasets from brown adipose tissue of cold exposed mice (Sustarsic et al., 2018). Our meta-analysis screening identified Protein Phosphatase 1 Regulatory Subunit 3B (PPP1R3B), as the highest induced regulatory subunit of a protein phosphatase at 3 days, 1 week and 3 weeks of cold exposure and the third highest at 1 day of cold exposure (Suppl. Fig. 4A). We confirmed by WB and qPCR that PPP1R3B was elevated at the protein and mRNA level (Figure 5C, D) in cold exposed mice. We then investigated *Ppp1r3b* mRNA and protein expression across different mouse tissues, showing a high and selective expression of *Ppp1r3b* in brown adipose tissue and liver (Figure 5E and Suppl. Fig. 4B, C). Collectively, these data strongly suggests that PPP1R3B could have a role in the thermogenic response of brown adipose tissue. To understand the mechanism of action of PPP1R3B, we searched for its potential interacting partners. For that purpose, we used the Biogrid database (Breitkreutz et al., 2003) and found that among the 9 identified PPP1R3B interacting proteins, YY1 is the third candidate after PP1CA and PP1CC (Suppl. Fig. 4D, E). We then confirmed that YY1 interacts

with PPP1R3B in U2OS cells expressing constructs for HA- and Flag-tagged proteins respectively by anti-Flag immunoprecipitation and WB (Figure 5F). Since YY1 is localized in the nucleus, and to further support the mechanisms of action of PPP13RB in brown adipocytes, we looked at its intracellular localization. We found that PPP1R3B is localized in the nucleus of brown adipocytes, independent of cAMP signaling (Figure 5G). This experiment confirmed that PPP1R3B expression is increased upon FSK treatment at the protein level (Figure 5G).

PPP1R3B does not harbor a phosphatase catalytic activity, it acts by directly regulating the Protein Phosphatase 1 (Mehta et al., 2017). We therefore asked whether PP1 function could impact on the YY1 phosphorylation status. To answer this question, we blocked the enzymatic activity of PP1 using okadaic acid (OA) in brown adipocytes. We found that the forskolin-dependent reduction of YY1 phosphorylation is blocked by OA treatment in brown adipocytes, suggesting that PP1 catalyzes YY1(S120) dephosphorylation (Figure 5H). PPP1R3B controls PP1 activity in the liver in the context of glycogen synthase (GS) and glycogen phosphorylase (GP) phosphorylation (Mehta et al., 2017). To understand the functional interaction between PPP1R3B and YY1 phosphorylation status, we performed a luciferase assay of *Ucp1* transcriptional activity by co-transfecting YY1 and PPP1R3B. Our results showed that PPP1R3B expression inhibits the YY1-dependent activation of *Ucp1* (Figure 5I).

Ppp1r3b loss-of-function _in vivo_ protects against diet-induced obesity.

To understand how PPP1R3B affects brown adipocyte thermogenesis, we generated both *Ppp1r3b* knockdown and overexpressing stable brown adipocytes. Our results show that UCP1 expression is increased at both RNA and protein level upon loss of *Ppp1r3b* (Figure 6A-B), but *Ucp1* levels remains unchanged when *Ppp1r3b* levels increase (Figure 6C). To investigate the physiological contribution of PPP1R3B in whole-body energy homeostasis, we used Antisense Oligos (ASOs) targeting *Ppp1r3b* or scramble control. *Ppp1r3b* expression

was reduced in brown adipose tissue by 66% (Figure 6D). Interestingly, core body temperature was elevated by 0.5ºC in *Ppp1r3b* knockdown mice compared to control, suggesting an increased energy expenditure (Figure 6E). We then challenged aso-CTR or aso-PPP1R3B mice with a HFD for 10 weeks and *Ppp1r3b* knockdown showed a protection against diet-induced obesity. While aso-CTR mice gain around 40% weight at 10 weeks since the start of HFD, aso-PPP1R3B only gained less than 20% (Figure 6F-H). Importantly, this phenotype was due to a decreased in total fat mass in aso-PPP1R3B mice (13% fat) compared to control (23) without changes in lean mass as shown by MRI measurements (Figure 6I-J). This was corroborated by the reduced weight of visceral and subcutaneous adipose depots (Figure 6K, L). Furthermore, glucose homeostasis was improved in HFD fed mice upon *Ppp1r3b* knockdown measured by glucose tolerance test (Figure 6M, N). In addition, total plasmatic triglycerides were reduced in *Ppp1r3b*-knockdown mice (Figure 6O). The improved metabolic homeostasis of *Ppp1r3b* knockdown mice on HFD was associated with a strong reduction of gene expression of key fatty acid synthesis enzymes in brown adipose tissue including *Acly*, *Acc1* and *Fasn* without changes in *Pparg* expression (Figure 6P).

DISCUSSION.

Our data show that YY1 orchestrates the sensing of energetic environmental stimuli through its S120 phosphorylation status in adipose tissues. Cold exposure and cAMP signaling leads to S120 dephosphorylation while high-fat diet feeding increases YY1(S120) phosphorylation. Cold exposure and HFD feeding are antagonistic stimuli that would trigger opposite downstream energetic and cellular responses. YY1(S120) dephosphorylation directly controls thermogenic response through the transcriptional regulation of *Ucp1*. Our RNAseq and GSEA data show that YY1 dephosphorylation activates several catabolic pathways while it represses several anabolic ones. AMPK and mTOR signaling pathways are also regulated upon YY1 phosphorylation status, suggesting that YY1(S120) phosphorylation status has a

control over these upstream pathways. The activation of pAMPK signaling upon YY1(S120) dephosphorylation supports the activation of a catabolic response. Although mTOR signaling is also activated, our data show that YY1(S120) dephosphorylation leads to a decreased expression of downstream signaling components of mTOR (including p70S6K, and regulators of ribosome function). Hence, the reduced levels of downstream targets of mTOR would result in a malfunctional compensatory hyperactivation of mTOR signaling. In agreement with this observation, a previous study showed that mTOR signaling is increased upon thermogenesis (Liu et al., 2016). Taken together, our results show that YY1 phosphorylation controls a switch between anabolic and catabolic status in brown adipocytes.

Multiple transcription factors or co-activators are known to control nutrient sensing and metabolism and the robustness of gene expression regulation is maintained through transcription factor redundancy (Kvon et al., 2021). We suggest here that YY1 exerts a basal but necessary layer of transcriptional regulation for specific metabolic transcription factors. The combined analysis of ChIPseq and RNAseq data has revealed two modes of YY1-dependent transcriptional control. On one hand we identify a canonical control through the binding of YY1 to the TSS of its putative targets. The regulation of gene expression is performed independently of YY1 recruitment but depends only on the S120 phosphorylation status. In this group of targets (that we named class A), we show that YY1(S120) phosphorylation plays an activating and repressive function since YY(S120A) leads to down- and upregulation of direct target genes shown by ChIPseq binding (Figure 3H-I). The localization of the S120 in the transactivation domain suggests that the activator and repressor roles are mediated by the interaction with specific chromatin factors. Among the directly downregulated genes by YY1(S120) dephosphorylation, we showed that ribosome and translation genes are overrepresented. This supports the maintenance of anabolic gene expression under YY1(S120) phosphorylated status. A recent finding identified the translation initiation factor eIF4E in promoting lipid metabolic processing and storage (Conn et al., 2021). YY1 has also been recently associated with translational control in the context of neural crest

development and melanoma formation (Varum et al., 2019). Our data are in agreement with these studies showing a translational control of lipid metabolism and anabolism.

On the other hand, we have identified a second class of target genes (class B) where YY1 binding is increased by the FSK mediated YY1(S120) dephosphorylation. The binding sites of this class of genes tend to be located at distant positions related to TSS. We have identified for example strongly regulated binding sites at *Adcy3* or *Prkar2b* located at +19 Kb and –39 Kb of TSS respectively. Gray et al. have previously shown that YY1 regulates promoter-enhancer loops in a CTCF-independent manner by forming YY1/YY1 homodimers (Weintraub et al., 2017). Our data analysis shows the distant YY1 binding sites located in *Adcy3* and *Prkar2b* interact with their respective TSS in agreement with the known promoter-enhancer function of YY1. Interestingly, both *Adcy3* and *Prkar2b* are genes involved in the canonical cAMP signaling pathway by promoting cAMP formation and activating PKA respectively. This suggests that YY1(S120) dephosphorylation induces a positive feedback loop by promoting the direct expression of at least *Prkar2b* which enhances adrenergic signaling.

We have in addition identified the upstream regulators of YY1 phosphorylation status. First, CK2 was an obvious candidate based on the identified consensus site and the previous published work (Riman et al., 2012). We confirmed here that YY1 is phosphorylated by CK2 also in brown adipocytes. A recent phosphoproteomic screening approach by Shinoda et al. identified CK2 as a regulator of thermogenesis (Shinoda et al., 2015). In this study, CK2 activity was found to be decreased upon adrenergic stimulation in adipocytes. Genetic or pharmacological inhibition of CK2 in mice led to increased expression of UCP1 in adipose tissue (Shinoda et al., 2015). This was associated with increased energy expenditure, improved insulin resistance and reduction of diet-induced obesity (Shinoda et al., 2015). In agreement with these data, we showed that CK2 inhibition leads to increased UCP1 levels in brown adipocytes. Shinoda et al. suggest that CK2 phosphorylates class I HDACs (HDAC1 and HDAC2), leading to the repression of genes involved in energy expenditure and thermogenesis. Our data add now a mechanism controlled by the transcription factor YY1.

First, the reduction of CK2 activity decreases YY1 phosphorylation and second, unphosphorylated YY1(S120) activates *Ucp1* expression. This suggests YY1 as a key direct transcriptional regulator of this process. We have observed a constitutive interaction of YY1-HDAC1 that is independent of adrenergic stimulation (Suppl. Fig. 3F), suggesting that the transcriptional activity controlled by the complex YY1-HDAC1 is mediated by CK2 activity through the phosphorylation of both YY1 and HDAC1. Upon a cAMP-dependent reduction of CK2 activity, *Ucp1* and other energy expenditure gene targets are activated.

In addition to CK2, our work revealed a novel regulator of YY1 phosphorylation status and energy balance. PPP1R3B was identified through an unbiased metanalysis screening where we looked specifically at phosphatases and their regulatory subunits. PPP1R3B is a regulatory phosphatase subunit of the phosphatase PP1. The holoenzyme PP1 regulates diverse cellular processes by controlling multiple targets through its catalytic activity subunit PPP1c (Moorhead et al., 2007). PPP1 regulatory subunits (PPP1Rs), a family of 7 members (PPP1RA-G), confer substrate specificity and regulate positive or negatively PP1 catalytic activity. We identified here the subunit PPP1R3B as highly induced by cold exposed mice in brown adipose tissue. Its expression is in addition exclusively restricted to brown adipose tissue and liver. A previous study has shown increased PPP1R3B in UCP1 expressing beige adipocytes within subcutaneous white adipose tissue upon CL treatment in mice (Wang et al., 2016). The role of PPP1R3B in thermogenesis is unknown. Our data shows a control of YY1 phosphorylation status by PPP1R3B that impacts whole-body energy balance. YY1-PPP1R3B interaction inhibit PP1 phosphatase activity thereby maintaining YY1(S120) phosphorylation. PPP1R3B has been reported to play a similar mechanism of action is by interacting with glycogen phosphorylase, an important regulatory mechanism promoting liver glycogen synthesis. Glycogen accumulation in brown adipose tissue has also been observed (Carmean et al., 2013). Whether PPP1R3B could affect glycogen metabolism in brown adipose tissue remains to be explored. Our data suggests that effects of PPP1R3B in systemic metabolism are mediated by targeting YY1 function. Mechanistically, PPP1R3B

controls YY1 phosphorylation status and thereby regulates YY1 dependent metabolic gene program. The cold-dependent upregulation of PPP1R3B seems to be contradictory given that its downregulation results in UCP1 overexpression. However, PPP1R3B is only upregulated after chronic cold exposure. We interpret these findings as a negative feedback loop, restoring YY1 phosphorylation and thereby breaking exacerbated catabolism and thermogenesis. In agreement with this hypothesis, we identified a YY1-dependent regulatory positive feedback loop of the adrenergic signaling cascade caused by the genomic control of *Adcy3* and *Prkar2b*. In this respect, the induction of PPP1R3B expression would attenuate the positive feedback loop of adrenergic signaling by restoring YY1 phosphorylation.

We show that the expression of PPP1R3B in brown adipose tissue has a systemic effect on adiposity and glucose homeostasis. It is possible that the glycogen metabolism in the liver may contribute to these effects, since *Ppp1r3b* expression is decreased in this tissue upon aso-PPP1R3B. However, a previous report showed no significant weight difference between a liver-specific *Ppp1r3b* mouse model compared to wildtype (Mehta et al., 2017), indicating that the changes in body weight composition that we observe are specifically mediated by the decreased expression of *Ppp1r3b* in brown adipose tissue.

In conclusion, our work has identified PPP1R3B as a novel signaling component that regulates whole-body energy balance by controlling the transcriptional activity and gene program of YY1. A phosphorylation switch of YY1 orchestrates opposite metabolic functions by exerting differential genomic and chromatin properties.

MATERIAL AND METHODS

Cell culture and reagents

Immortalized brown adipocyte cell lines, pBAT and De23 were grown at 37°C in 5% CO2 in Dulbecco's Modified Eagle Medium: Nutrient Mixture F-12 (DMEM/F-12) supplemented with 10% fetal bovine serum and and 1% penicillin-streptomycin. Adipogenic differentiation was induced upon confluency by supplementing the media with 500μM methyl isobutyl xanthine (IBMX) (Sigma Aldrich, I5879), 5μM dexamethasone (Sigma Aldrich, D4902), 20nM insulin (Sigma Aldrich, I0516), 1nM T3 (Sigma Aldrich, T6397) and 1μM Rosiglitazone (Sigma Aldrich, T2408). After 48 hours, medium was replaced with maintaining medium containing insulin and T3. Maintaining media was changed every 2 days for a total of 4 to 6 days. For cAMP induction, differentiated cells were treated with FSK (Fisher Bioreagents, BP2520-10) at 10 μM for a maximum of 4h, DMSO used as a control. To investigate CK2 involvement in YY1 phosphorylation, differentiated cells were treated with the inhibitor 4,5,6,7-Tetrabromobenzotriazole (TBB) (Tocris Bioscience, 2275) at 50 μM for 15 min and FSK at 10 μM for 30 minutes, DMSO as a control treatment. For phosphatase 1 (PP1) inhibition assay, differentiated brown adipocytes were treated with Okadaic acid (OA) (Cell signaling, 5934S) at 5 nM for 1 hour followed by FSK treatment at 10 μM for 1 hour and DMSO as a control.

Protein extraction and western blot

Differentiated adipocytes were homogenized in RIPA buffer (50 mM Tris pH 8.0, 150 mM NaCl, 1% NP-40, 0.5% sodium Deoxicholate and 0.1% SDS) supplemented with phosphatase inhibitor (Cell signaling, 5870S) and protease inhibitor cocktails (Roche, Complete 11873580001) for 15 minutes. Lysates were centrifugated 12,000g for 15 minutes and the supernatant was collected. Protein quantification was determined with BCA Protein Assay Kit (Thermo Fischer, 23225). Proteins, 30–40 μg, were separated in 10% SDS-

acrylamide gels and transferred to PVDF membranes (Millipore). Phospho-specific YY1 S120 antibody was obtained from Dr. Raed Rizkallah. UCP1 (ab10983), PPP1R3B (ab235049) and HA (ab9110) antibodies were purchased from Abcam. The antibodies for GAPDH (G8795), Tubulin (T6199) and FLAG (F3165) were obtained from Sigma Aldrich. The antibody for YY1 (46395) and LAMIN (14-9688-80) were purchased from Cell Signaling and Invitrogen respectively. HRP-conjugated anti-mouse (31431) and anti-rabbit (31466) from thermo fisher were used as secondary antibodies.

Cloning and cell lines generation.

Generation of YY1 point mutants at position S120 was carried out by using PCR-based site directed mutagenesis with the following primers: for YY1-S120A forward 5'-CAGCCCGTCCGCGTCGTCCCCGC-3' and reverse 5'-GCGGGGACGACGCGGACG-GGCTG-3'; for YY1-S120E forward 5'-GCAGCCCGTCCTCGTCGTCCCCG-3' and reverse 5'-CGGGGACGACGAGGACGGGCTGC-3'. *Ppp1r3b* (Myc-DDK-tagged) coding region was amplified from a *Ppp1r3b* pCMV6 vector (NM_177741, CAT#: MR203867, Origene) and cloned into pBABE retroviral vector. *Ppp1r3b* shRNA sequence KD1: forward 5'-CCGGACACACTGGCCTGATTGATACCTCGAGGTATCAATCAGGCCAGTGTGTTTTTTG-3' and reverse 5'- AATTCAAAAAACACACTGGCCTGATTGATACCTCGAGGTATCAATCA-GGCCAGTGTGT-3'; KD2: forward 5'-CCGGCAGATTTCCCTTGTCAGTATGCTCGAGCAT-ACTGACAAGGGAAATCTGTTTTTG-3' and reverse 5'-AATTCAAAAACAGATTTCCCTTG-TCAGTATGCTCGAGCATACTGACAAGGGAAATCTG-3'. shRNAs were cloned into pLKO.1-blast plasmid (Addgene, #26655) and co-transfected with psPAX2 and pMD2.G plasmids for virus production. pLKO.1-blast scramble (Addgene, #26701) was used as control. All plasmids were verified by sequencing. HEK293T cells were used for lentivirus and retrovirus packaging. For the generation of stable cell lines, pre-adipocytes De23 cells were infected with viral constructs in the presence of polybrene and selected with puromycin 2,5 μg/mL (Sigma, P8833) or blasticidin 10 μg/mL (Thermofisher, A1113902).

Oxygen consumption assay

The Oxygen Consumption Rate (OCR) and extracellular acidification rate (ECAR) were measured in differentiated brown adipocytes using a Seahorse Extracellular flux analyzer XFp (Agilent). Basal respiration levels were measured followed by the addition of 5μM oligomycin (Calbiochem, 495455) to determine ATP-coupled respiration and the maximal respiration was obtained after the addition of 1 μM FCCP (Sigma Aldrich, C2920). Finally, 5 μM antimycin A (Sigma Aldrich, A8674) and rotenone (Sigma Aldrich, R8875) were added to inhibit mitochondrial respiration.

Kinase assays

For cold kinase assays pre-adipocytes were transfected with Flag tagged YY1 mutants for overexpression. Flag-YY1 mutants were purified with Flag M2 Affinity Agarose Gel (Sigma Aldrich, A2220) and subsequent eluted with Flag peptides (Sigma Aldrich, F3290). For GST-YY1 constructs, BL21 *E. coli* bacteria were transfected with GST–YY1 constructs, both in full length mutants and truncated YY1 following Glutathione sepharose beads (GE Healthcare, 17-0756-01) purification. GST-YY1 constructs were used for cold and hot kinase assays. Kinase reactions for the cold kinase assay were performed using purified Casein Kinase II (CKII) (NEB, P6010) in CK II kinase buffer (NEB, P6010) supplemented with 2mM of cold ATP for 30 min at 30°C. For the hot kinase assay, reactions were performed as described above but supplemented with 50 μM of cold ATP and 0.25 μM [γ-^{32}P]ATP. Reactions were then stopped by the addition of SDS-PAGE buffer and loaded for separation on a 10% SDS-PAGE gel.

Immunoprecipitation

For co-immunoprecipitation, U2OS cells were transiently transfected with 1 μg of pCDNA3.1 HA-YY1, pCMV6 FLAG-PPP1R3B or control empty plasmid and harvested 48hrs after transfection. Briefly, samples were lysed in IP buffer (Hepes 20 mM pH 7.9, NaCl 125 mM, Chaps 0.3% and EDTA 1mM), supplemented with protease inhibitor cocktail (Roche, Complete 11873580001) for 15 minutes followed by centrifugation at 18,000 g at 4ºC to pellet debris. Supernatants were collected and incubated with FLAG M2 Affinity Agarose Gel beads (Sigma Aldrich, A2220) 16h at 4ºC. Beads were washed using IP buffer four times. Immunoprecipitates and total cell lysates were heated at 95°C in SDS loading buffer for 15 minutes and then subjected to Western blot analysis.

Gene expression analysis

Total RNA was extracted using TRI Reagent (MRC, TR118) and reverse-transcribed using the High-Capacity cDNA Reverse Transcription kit (Applied Biosystems) according to the manufacture's protocol. Quantitative RT-PCR was performed using SYBR green master mix on the QuantStudio™ 5 - 384-Well Block instrument (Thermo fisher). Reactions were carried out in triplicate and relative differences in gene expression were normalized to the expression levels of the housekeeping genes *36b4* or *Rpl13* by using the standard curve method. Primers sequences are available in supplementary data.

For RNA sequencing analysis, RNA was extracted as described above and used to construct libraries (TruSeq 2, Illumina) according to the user's instruction manual. NovaSeq platform was utilized to generate 100-bp paired-end sequencing reads (400 M reads).

Chromatin immunoprecipitation and sequencing.

Differentiated adipocytes were cross-linked for 10min with 1% formaldehyde in PBS, followed by nuclear isolation and sonication. Samples were sonicated for 10 cycles 30" ON, 30" OFF at 4 °C using a Bioruptor Pico sonicator. Sheared chromatin was incubated with specific antibodies against YY1 (Cell signaling, 46395), YY1 pS120 (obtained from Dr. Raed Rizkallah),

H3 (Abcam, ab1791) or IgG (Thermo fisher, 31466) followed by immunoprecipitation with protein G dynabeads (Thermo fisher, 10003D). DNA was purified by reverse cross-linking and phenol-chloroform extraction.

ChIPseq analysis.

Sequencing reads were normalized using the SpikeIn control, mapped for the mouse genome (version mm10) and selected for unique reads with BWA (mem default parameters) and SAMTOOLS respectively (skipping alignments smaller than 10bp). YY1 binding peaks were identified with MACS2 using input samples as reference control. Differential binding occupancy was performed with MACS2 and HOMER. We used Chipseeqer and clusterProfiler for the pathway enrichment analysis of identified peaks and DEEPTOOLS for plotting heatmaps of binding using the indicated reference matrix.

Hi-C analysis.

The Hi-C Summary Format file for Day 2 was downloaded from the NCBI (GSM2515986) website. The data was first converted from mm9 to mm10 with mm9ToMm10.over.chain file using the R liftOver tool. Then HOMER (Heinz S. et al.) was used to build a tag directory (makeTagDirectory -format HiCsummary with parameters --tbp 1 -removePEbg -removeSpikes 10000 5 -genome mm10). The prepared tag directory was used to extract the HiC contact matrix for the region of interest at chr12 using a resolution of 5 Kb and a 50 Kb moving window (analyzeHiC function with parameters -res 5000 –superRes 50000, as it was done in the original study (Siersbæk et al., 2017)). To find significant interactions on the chr12, we used the analyzeHiC function (-interactions specification) with the following parameters: -chr chr12 -res 5000 -superRes 50000 -pvalue 0.01. The output yielded a table of pairwise interactions that passed 0.01 p-value threshold, and the corresponding statistics including FDR (False Discovery Rate based on Benjamini correction) and logP (natural logarithm of the p-value for the interaction), etc. This matrix of significant pairwise

interactions was further filtered by setting the 0.01 FDR threshold. Only the interactions that passed the thresholds were used for visualization of the arc plot, where a greater thickness of arcs, as well as a greater intensity of colors, corresponds to a more significant p-value.

Animals

All mice used in this study were male on a C57BL6/J background maintained on standard chow diet or fed a 60% high fat diet (HFD) (Kliba-Nafag, #2127) for 1-12 weeks. Mice were 8 to 10 weeks old when placed on HFD. Blood was collected by cardiac puncture. Tissue for protein or RNA extraction was homogenized with metal beads using a TissueLyser (Qiagen) with 15 minutes of lysis at a frequency of 25s in RIPA buffer for protein (50 mM Tris pH 8.0, 150 mM NaCl, 1% NP-40, 0.5% sodium Deoxicholate and 0.1% SDS), supplemented with phosphatase inhibitor (Cell signaling, 5870S) and protease inhibitor cocktails (Roche, Complete 11873580001) or TRIZOL reagent (Thermofisher, 15596026) for RNA.

***Ppp1r3b* knock-down in vivo**

Mice were subcutaneously injected in the neck with 50 mg/Kg once per week with antisense oligonucleotides directed to *Ppp1r3b* (CTCAAATCTGGCCGGG) or a vehicle control (ASOS, Ionis). The mice were maintained in chow diet for 4 weeks or HFD for 10 weeks. Weight was monitored weekly. 48 hours after last injection, animals were euthanized, and tissues harvest as described above.

Body temperature and body composition

Body temperatures of mice (basal metabolic state) were taken using a rectal probe (Bioseb) after 4 weeks of ASOs injections fed regular chow. After 9 weeks of HFD, total body composition of the mice was analyzed by performing an EchoMRI (EchoMRI™ whole body composition analyzer).

Glucose tolerance test

Mice were fasted for 16 hours overnight. After measuring basal fasting blood glucose, 0,2g/ml glucose solution was injected intraperitoneally (1g/kg). Blood was collected from an incision at the tip of the tail. Glucose concentration was measured at 20, 40, 60, 100 and 120 minutes using a StatStrip Xpress Glucometer (Nova Biomedical).

Triglyceride quantification

Blood samples were centrifuged at 2,000 g for 10 min. Serum was collected and stored at −80°C for further analysis. Triglycerides were determined using GPO TG kit from Beckman Coulter System SYNCHRON.

Dual-luciferase reporter assay

Immortalized brown adipocytes De23 cell lines were co-transfected using Lipofectamine2000 with plasmid expressing Flag-YY1, Flag-YY1(S120A), Flag-Ppp1r3b, (Origene, MR203867), *Ucp1*-luciferase reporter plasmids E1 and Renilla as an internal control vector. All the plasmids were constructed in a pcDNA3*Ucp1*-luciferase reporter plasmid E1 (up to -3.3 Kb from the translation initiation site chr8:85,811,258-85,814,509) was kindly provided by the Sakai lab and constructed in a pGL3-basic vector (Abe et al., 2015). Luciferase assay was performed 48 hours after transfection using the Dual-Luciferase® Reporter Assay System (Promega, #E1910) according to the manufacturer's instructions. Luminescence signal was detected with the Tecan-I control machine and normalized to Renilla signal. All luciferase assay data represent ± SEM of triplicate samples.

FIGURE LEGENDS.

Figure 1. YY1(S120) dephosphorylation in brown adipocytes induces thermogenesis. A) YY1 domains configuration and S120 phosphorylation. **B)** WB analysis of brown adipose tissue (BAT) isolated from mice at room temperature (RT) (22°C) or exposed to cold (6 °C) for 4 and 12 hours. **C)** Time course of YY1(S120) phosphorylation in response to FSK (10 μM) versus DMSO control in differentiated pBAT brown adipocytes**. D,E)** YY1(S120) phosphorylation of BAT and Inguinal White Adipose Tissue (IWAT) samples from chow or HFD fed mice for 1 and 12 weeks, respectively. **F)** UCP1 expression in differentiated brown adipocytes stably expressing GFP control, 3X-Flag-YY1, 3X-Flag YY1(S120A) or 3X-Flag-YY1(S120E). **G)** Relative mRNA expression of brown adipocyte target genes versus reference gene *Rpl13* in YY1-wildtype versus YY1(S120A) and YY1(S120E) brown adipocytes. **H)** Oxygen consumption rate (OCR) measured at the basal level followed by the addition of oligomycin (5 μM), FCCP (1 μM), and antimycin A and rotenone (5 μM) using a Seahorse® Device. For G and H n= 3, error bars indicate SEM. Statistically significant differences shown by Student t-test *** p-value <0.001,** p-value <0.01 and * p-value <0.05. Western blot detection was performed using specific antibodies and GAPDH or Tubulin were taken as a control.

Figure 2. YY1 phosphorylation controls a catabolic/anabolic switch in brown adipocytes. A) Volcano plot of RNA-seq analysis of control wildtype YY1 versus YY1(S120A) expression in brown adipocytes. In red significant upregulated genes, in significant down-regulated genes and grey no significant genes. Vertical dotted lines are positioned at a log2

fold-change of 1 or −1 and horizontal dotted lines are positioned at the equivalent of p<0.05 **B)** KEGG enrichment analysis displaying upregulated biological pathways and **C)** downregulated biological pathways . **D)** GSEA showing positive and negative MES values indicating overexpressed and downregulated pathways respectively and selection of relevant pathways. **E)** WB of AMPK and mTOR signaling from YY1 wildtype versus YY1(S120A) De23 brown adipocytes. WB detection was performed with the indicated specific antibodies and Tubulin as a loading control.

Figure 3. Genome-wide binding of YY1 in brown adipocytes in response to adrenergic signaling. A) Heatmap showing YY1 binding spanning 10 Kb of TSS across whole genome in DMSO or FSK stimulated brown adipocytes (De23). **B)** Genomic feature distribution of YY1 binding and identified DNA binding motif. **C)** KEGG pathway enrichment analysis of the nearest genes to YY1 binding loci in CTR and FSK respectively. **D)** Genome browser ChIPseq tracks of YY1 binging at the *Ucp1* locus in CTR versus FSK. **E)** ChIP-qPCR relative enrichment of YY1 and **F)** YY1(pS120) at the *Ucp1* enhancer region and *Cyc* promoter or *Acta2* as positive and negative control respectively. **G)** Luciferase reporter assay driven by *Ucp1* promoter and one enhancer element (E1) after transfection of Flag-YY1 or Flag-YY1(S120A). Signal was normalized to the Renilla reporter vector. **H,I)** Heatmap showing YY1 binding sites in DMSO or FSK stimulated brown adipocytes on TSS of genes up or downregulated identified by RNA-seq data. Error bars indicate SEM. Statistically significant differences shown by Student t-test or one-way ANOVA *** p-value <0.001,** p-value <0.01 and * p-value <0.05.

Figure 4. Differential YY1 genomic binding upon FSK treatment and identification of *Prakar2b* and *Adcy3* loci.

A) Heatmap showing YY1 differential binding sites in DMSO or FSK stimulated brown adipocytes. **B)** Genomic distribution of differential binging sites of annotated chromatin regions

identified in ChIP-seq data sets and MEME motif discovery analysis. **C)** Genome browser ChIP-seq tracks of YY1 binging at the *Prkar2b* locus. **D)** *Prkar2b* Relative mRNA expression in differentiated brown adipocytes stably expressing wildtype 3XFlag-YY1 or 3XFlag YY1(S120A) versus reference gene *Rpl13.* Error bars indicate SEM. Statistically significant differences shown by Student t-test * p-value <0.05. **E)** *Prkar2b* locus showing Hi-C matrix, YY1 ChIPseq track and the arc plot with significant Hi-C interactions (p-value < 0.01).

Figure 5. Identification of CK2 and PPP1R3B as molecular regulators of YY1 S120 phosphorylation. A) In vitro cold kinase assay of GST-YY1 full length protein or GST-YY1 DNA binding domain with recombinant CK2 detected by WB with anti-YY1(pS120) antibody. **B)** WB of brown adipocytes treated with DMSO, FSK, TBB or FSK+TBB. Adipocytes were pretreated with TBB for 15min followed by FSK treatment for 30min before harvesting. **C)** Protein and **D)** Relative mRNA analysis of BAT isolated from mice at room temperature (RT) (22°C) or exposed to cold (6 °C) for 4 , 12 or 24 hours. **E)** PPP1R3B detection by WB in different mouse tissues. **F)** Co-immunoprecipitation of transfected Flag-PPP1R3B and HA-YY1 in U2OS cells, pulldown with anti-Flag antibodies and detected with anti-HA antibodies. **G)** Cytoplasmic and nuclear protein fractionation followed by WB with anti-YY1, anti-PPP1R3B and the indicated control antibodies. **H)** WB to detected YY1(S120) phosphorylation in brown adipocytes after Okadaic acid (OA) for 1 hour followed by forskolin addition for 1 hour before harvesting. **I)** Luciferase reporter assay driven by *Ucp1* promoter and one enhancer element (E1) after transfection with Flag-YY1 or FLAG-PPP1R3B. Signal was normalized to the Renilla reporter vector. WBs detection were performed using specific antibodies and GAPDH or Tubulin for loading control. Error bars indicate SEM. Student t-test statistically significant differences shown by and *** p-value <0.001,** p-value <0.01 and * p-value <0.05.

Figure 6. *Ppp1r3b* KD protects against diet-induced obesity. A) *Ucp1* and *Ppp1r3b* relative mRNA expression from brown adipocytes stably expressing shScramble or two different

shPpp1r3b (KD1 and KD2). **B)** WB of UCP1 of *shPpp1r3b* KD1 and KD2 brown adipocytes. **C)** *Ucp1* and *Ppp1r3b* relative mRNA expression from brown adipocytes overexpressing *Ppp1r3b* or control plasmid generated by lentiviral stable selection. **D)** *Ppp1r3b* relative mRNA expression of BAT of wildtype mice injected once a week subcutaneously with asoCTR or asoPPP1R3B. **E)** Rectal temperature of wildtype mice injected once a week subcutaneously with asoCTR or asoPPP1R3B for 4 weeks (n=12 mice). **F)** Representative images of asoCTR and asoPPP1R3B mice injected once per week subcutaneously for 10 weeks on HFD feeding. **G)** Total body weight and **H)** percentage of increased body weight of asoCTR or asoPPP1R3B mice on HFD (n=10). At week 9 of the HFD, whole body composition was analyzed by EchoMRI to determine **I)** fat mass and **J)** lean mass. **K)** Weights for IWAT and **L)** EWAT were measured at sacrifice. **M)** Intraperitoneal glucose tolerance test (GTT) in 16 h fasted mice after 9 weeks of HFD and ASOs injection. **N)** Area under the curve of M. **O)** Serum triglyceride levels of asoCTR vs asoPPP1R3B**. P)** Relative mRNA expression of some *de novo* lipogenesis genes in BAT of asoCTR and asoPPP1R3B HFD mice**.** Data represented means of 10 mice per group. Error bars indicate SEM. Statistically significant differences shown by Student t-test *** p-value <0.001,** p-value <0.01 and * p-value <0.05. Western blot detection was performed using specific antibodies and Tubulin for loading control.

REFERENCES.

Abe, Y., Rozqie, R., Matsumura, Y., Kawamura, T., Nakaki, R., Tsurutani, Y., Tanimura-Inagaki, K., Shiono, A., Magoori, K., Nakamura, K., et al. (2015). JMJD1A is a signal-sensing scaffold that regulates acute chromatin dynamics via SWI/SNF association for thermogenesis. Nat. Commun.

Blättler, S.M., Cunningham, J.T., Verdeguer, F., Chim, H., Haas, W., Liu, H., Romanino, K., Rüegg, M.A., Gygi, S.P., Shi, Y., et al. (2012). Yin Yang 1 deficiency in skeletal muscle protects against rapamycin-induced diabetic-like symptoms through activation of insulin/IGF signaling. Cell Metab. *15*.

Blondin, D.P., Nielsen, S., Kuipers, E.N., Severinsen, M.C., Jensen, V.H., Miard, S., Jespersen, N.Z., Kooijman, S., Boon, M.R., Fortin, M., et al. (2020). Human Brown Adipocyte Thermogenesis Is Driven by β2-AR Stimulation. Cell Metab.

Bonet, M.L., Mercader, J., and Palou, A. (2017). A nutritional perspective on UCP1-dependent thermogenesis. Biochimie *134*, 99–117.

Breitkreutz, B.J., Stark, C., and Tyers, M. (2003). The GRID: the General Repository for Interaction Datasets. Genome Biol.

Cannon, B., and Nedergaard, J. (2004). Brown Adipose Tissue: Function and Physiological Significance. Physiol. Rev. *84*, 277–359.

Carmean, C.M., Bobe, A.M., Yu, J.C., Volden, P.A., and Brady, M.J. (2013). Refeeding-Induced Brown Adipose Tissue Glycogen Hyper-Accumulation in Mice Is Mediated by Insulin and Catecholamines. PLoS One *8*, e67807.

Chouchani, E.T., Kazak, L., and Spiegelman, B.M. (2019). New Advances in Adaptive Thermogenesis: UCP1 and Beyond. Cell Metab. *29*, 27–37.

Cohen, P., and Kajimura, S. (2021). The cellular and functional complexity of thermogenic fat. Nat. Rev. Mol. Cell Biol. 1–17.

Conn, C.S., Yang, H., Tom, H.J., Ikeda, K., Oses-Prieto, J.A., Vu, H., Oguri, Y., Nair, S., Gill, R.M., Kajimura, S., et al. (2021). The major cap-binding protein eIF4E regulates lipid

homeostasis and diet-induced obesity. Nat. Metab. *3*, 244–257.

Cypess, A.M., Weiner, L.S., Roberts-Toler, C., Elía, E.F., Kessler, S.H., Kahn, P.A., English, J., Chatman, K., Trauger, S.A., Doria, A., et al. (2015). Activation of human brown adipose tissue by a β3-adrenergic receptor agonist. Cell Metab.

Eguchi, J., Wang, X., Yu, S., Kershaw, E.E., Chiu, P.C., Dushay, J., Estall, J.L., Klein, U., Maratos-Flier, E., and Rosen, E.D. (2011). Transcriptional Control of Adipose Lipid Handling by IRF4. Cell Metab. *13*, 249–259.

Feige, J.N., and Auwerx, J. (2007). Transcriptional coregulators in the control of energy homeostasis. Trends Cell Biol. *17*, 292–301.

Giannopoulou, E.G., and Elemento, O. (2011). An integrated ChIP-seq analysis platform with customizable workflows. BMC Bioinformatics.

Giordano, A., Frontini, A., and Cinti, S. (2016). Convertible visceral fat as a therapeutic target to curb obesity. Nat. Publ. Gr. *15*.

González, A., Hall, M.N., Lin, S.C., and Hardie, D.G. (2020). AMPK and TOR: The Yin and Yang of Cellular Nutrient Sensing and Growth Control. Cell Metab. *31*, 472–492.

Gordon, S., Akopyan, G., Garban, H., and Bonavida, B. (2006). Transcription factor YY1: structure, function, and therapeutic implications in cancer biology. Oncogene *25*, 1125–1142.

Hardie, D.G., Schaffer, B.E., and Brunet, A. (2016). AMPK: An Energy-Sensing Pathway with Multiple Inputs and Outputs. Trends Cell Biol. *26*, 190–201.

Hornbeck, P. V., Zhang, B., Murray, B., Kornhauser, J.M., Latham, V., and Skrzypek, E. (2015). PhosphoSitePlus, 2014: Mutations, PTMs and recalibrations. Nucleic Acids Res.

Kusminski, C.M., Bickel, P.E., and Scherer, P.E. (2016). Targeting adipose tissue in the treatment of obesity-associated diabetes. Nat. Rev. Drug Discov. *15*, 639–660.

Kvon, E.Z., Waymack, R., Elabd, M.G., and Wunderlich, Z. (2021). Enhancer redundancy in development and disease. Nat. Rev. Genet.

Lefterova, M.I., Haakonsson, A.K., Lazar, M.A., and Mandrup, S. (2014). PPARγ and the global map of adipogenesis and beyond. Trends Endocrinol. Metab. *25*, 293–302.

Liu, D., Bordicchia, M., Zhang, C., Fang, H., Wei, W., Li, J.-L., Guilherme, A., Guntur, K., Czech, M.P., and Collins, S. (2016). Activation of mTORC1 is essential for β-adrenergic stimulation of adipose browning. J. Clin. Invest. *126*, 1704–1716.

Mehta, M.B., Shewale, S. V, Sequeira, R.N., Millar, J.S., Hand, N.J., and Rader, D.J. (2017). Hepatic protein phosphatase 1 regulatory subunit 3B (Ppp1r3b) promotes hepatic glycogen synthesis and thereby regulates fasting energy homeostasis. J. Biol. Chem. *292*, 10444–10454.

Mi, H., Muruganujan, A., Casagrande, J.T., and Thomas, P.D. (2013). Large-scale gene function analysis with the panther classification system. Nat. Protoc.

Moorhead, G.B.G., Trinkle-Mulcahy, L., and Ulke-Lemée, A. (2007). Emerging roles of nuclear protein phosphatases. Nat. Rev. Mol. Cell Biol. *8*, 234–244.

Mootha, V.K., Lindgren, C.M., Eriksson, K.F., Subramanian, A., Sihag, S., Lehar, J., Puigserver, P., Carlsson, E., Ridderstråle, M., Laurila, E., et al. (2003). PGC-1α-responsive genes involved in oxidative phosphorylation are coordinately downregulated in human diabetes. Nat. Genet.

Obenauer, J.C., Cantley, L.C., and Yaffe, M.B. (2003). Scansite 2.0: Proteome-wide prediction of cell signalling interactions using short sequence motifs. Nucleic Acids Res.

Puigserver, P., and Spiegelman, B.M. (2003). Peroxisome Proliferator-Activated Receptor-γ Coactivator 1α (PGC-1α): Transcriptional Coactivator and Metabolic Regulator. Endocr. Rev. *24*, 78–90.

Riman, S., Rizkallah, R., Kassardjian, A., Alexander, K.E., Luscher, B., and Hurt, M.M. (2012). Phosphorylation of the Transcription Factor YY1 by CK2 Prevents Cleavage by Caspase 7 during Apoptosis. Mol. Cell. Biol.

Rosen, E.D., and Spiegelman, B.M. (2014). What We Talk About When We Talk About Fat. Cell *156*, 20–44.

Sanchez-Gurmaches, J., and Guertin, D.A. (2014). Adipocyte lineages: Tracing back the origins of fat. Biochim. Biophys. Acta - Mol. Basis Dis. *1842*, 340–351.

Scheele, C., and Wolfrum, C. (2020). Brown Adipose Crosstalk in Tissue Plasticity and Human Metabolism. Endocr. Rev.

Shao, M., Ishibashi, J., Kusminski, C.M., Holland, W.L., Seale, P., Gupta Correspondence, R.K., Wang, Q.A., Hepler, C., Vishvanath, L., Macpherson, K.A., et al. (2016). Zfp423 Maintains White Adipocyte Identity through Suppression of the Beige Cell Thermogenic Gene Program Article Zfp423 Maintains White Adipocyte Identity through Suppression of the Beige Cell Thermogenic Gene Program. Cell Metab. *23*, 1167–1184.

Shinoda, K., Ohyama, K., Hasegawa, Y., Chang, H.Y., Ogura, M., Sato, A., Hong, H., Hosono, T., Sharp, L.Z., Scheel, D.W., et al. (2015). Phosphoproteomics Identifies CK2 as a Negative Regulator of Beige Adipocyte Thermogenesis and Energy Expenditure. Cell Metab. *22*, 997–1008.

Siersbæk, R., Madsen, J.G.S., Javierre, B.M., Nielsen, R., Bagge, E.K., Cairns, J., Wingett, S.W., Traynor, S., Spivakov, M., Fraser, P., et al. (2017). Dynamic Rewiring of Promoter-Anchored Chromatin Loops during Adipocyte Differentiation. Mol. Cell *66*, 420-435.e5.

Spiegelman, B.M., Seale, P., and Kajimura, S. (2009). Transcriptional control of brown adipocyte development and physiological function-of mice and men. Genes Dev.

Subramanian, A., Tamayo, P., Mootha, V.K., Mukherjee, S., Ebert, B.L., Gillette, M.A., Paulovich, A., Pomeroy, S.L., Golub, T.R., Lander, E.S., et al. (2005). Gene set enrichment analysis: A knowledge-based approach for interpreting genome-wide expression profiles. Proc. Natl. Acad. Sci. U. S. A.

Sustarsic, E.G., Ma, T., Lynes, M.D., Larsen, M., Karavaeva, I., Havelund, J.F., Nielsen, C.H., Jedrychowski, M.P., Moreno-Torres, M., Lundh, M., et al. (2018). Cardiolipin Synthesis in Brown and Beige Fat Mitochondria Is Essential for Systemic Energy Homeostasis. Cell Metab. *28*, 159-174.e11.

Varum, S., Baggiolini, A., Zurkirchen, L., Atak, Z.K., Cantù, C., Marzorati, E., Bossart, R., Wouters, J., Häusel, J., Tuncer, E., et al. (2019). Yin Yang 1 Orchestrates a Metabolic Program Required for Both Neural Crest Development and Melanoma Formation. Cell Stem Cell *24*,

637-653.e9.

Verdeguer, F., Soustek, M.S., Hatting, M., Blättler, S.M., McDonald, D., Barrow, J.J., and Puigserver, P. (2016). Brown adipose YY1 deficiency activates expression of secreted proteins linked to energy expenditure and prevents diet-induced obesity. Mol. Cell. Biol. *36*.

Wang, H., Liu, L., Lin, J.Z., Aprahamian, T.R., and Farmer, S.R. (2016). Browning of White Adipose Tissue with Roscovitine Induces a Distinct Population of UCP1+ Adipocytes. Cell Metab. *24*, 835–847.

Weintraub, A.S., Li, C.H., Zamudio, A. V, Sigova, A.A., Hannett, N.M., Day, D.S., Abraham, B.J., Cohen, M.A., Nabet, B., Buckley, D.L., et al. (2017). YY1 Is a Structural Regulator of Enhancer-Promoter Loops. Cell *171*, 1573-1588.e28.

Figure 1

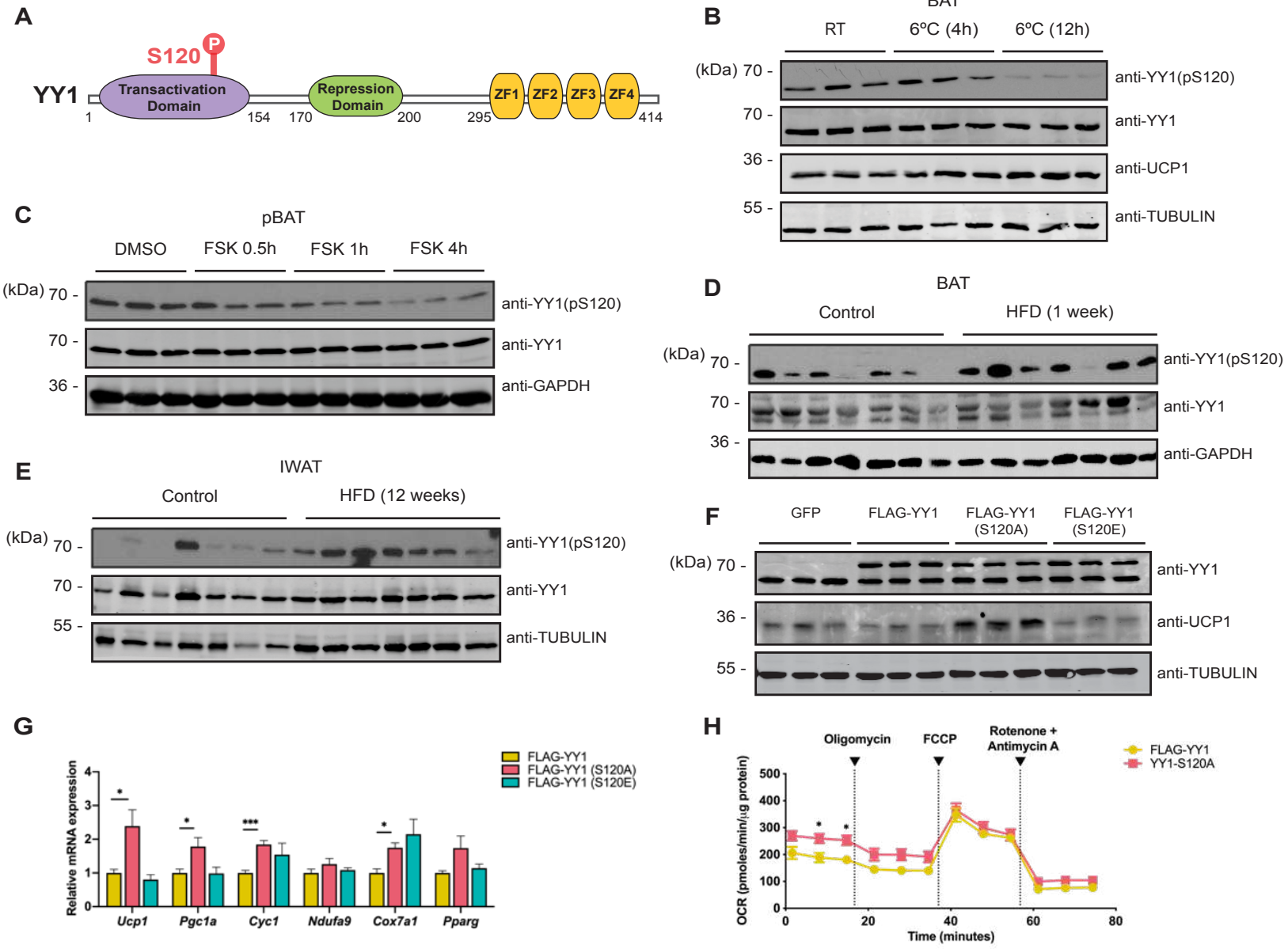
A
S120
P
YY1
Transactivation Domain
Repression Domain
ZF1
ZF2
ZF3
ZF4
1
154
170
200
295
414
B
BAT
RT
6ºC (4h)
6ºC (12h)
(kDa)
70 -
anti-YY1(pS120)
anti-YY1
36 -
anti-UCP1
55 -
anti-TUBULIN
C
pBAT
DMSO
FSK 0.5h
FSK 1h
FSK 4h
anti-GAPDH
D
Control
HFD (1 week)
E
IWAT
HFD (12 weeks)
F
GFP
FLAG-YY1
FLAG-YY1 (S120A)
FLAG-YY1 (S120E)
G
FLAG-YY1
FLAG-YY1 (S120A)
FLAG-YY1 (S120E)
Relative mRNA expression
Ucp1
Pgc1a
Cyc1
Ndufa9
Cox7a1
Pparg
H
Oligomycin
FCCP
Rotenone + Antimycin A
FLAG-YY1
YY1-S120A
OCR (pmoles/min/µg protein)
Time (minutes)

Figure 2

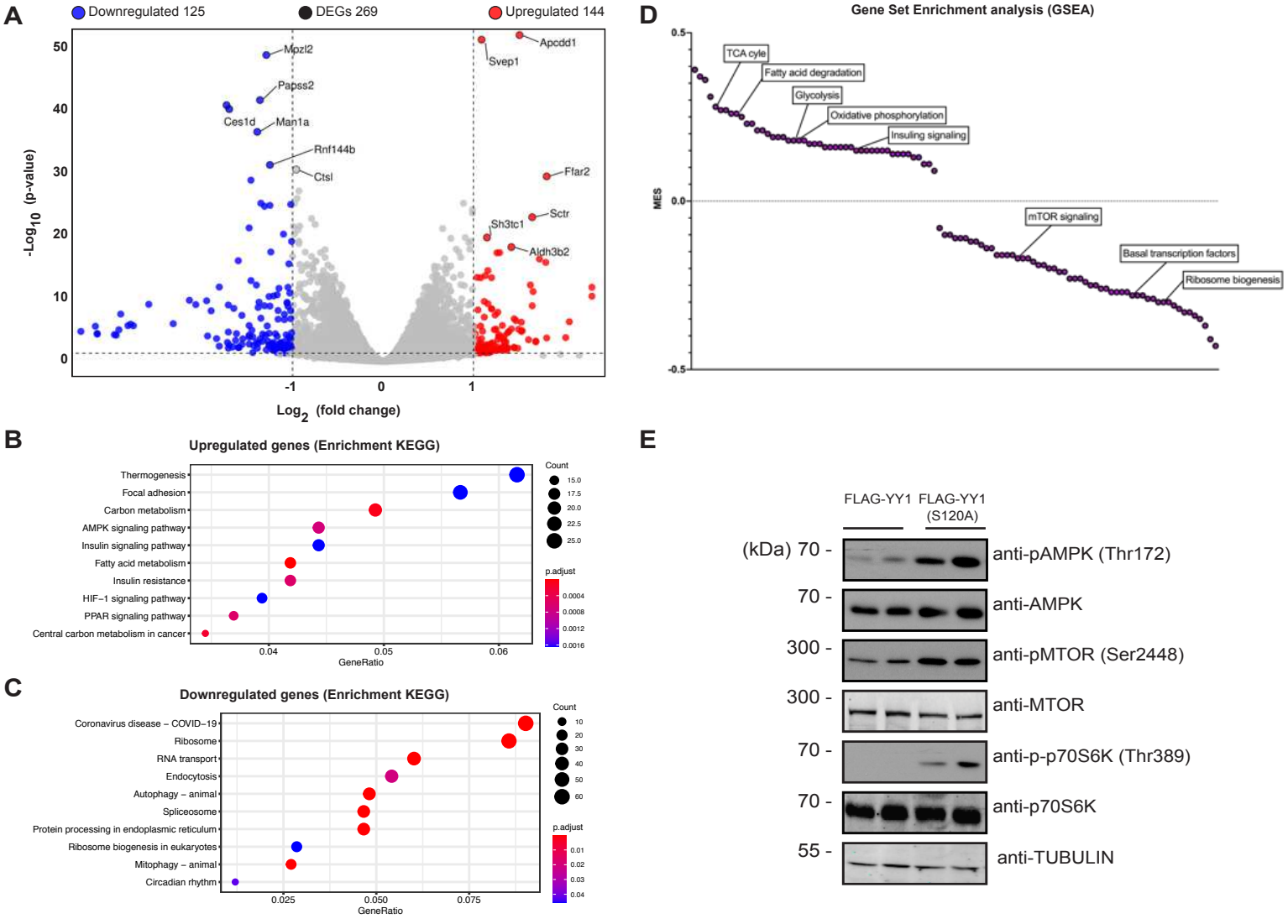
A
Downregulated 125
DEGs 269
Upregulated 144
Mpzl2
Papss2
Ces1d
Man1a
Rnf144b
Ctsl
Apcdd1
Svep1
Ffar2
Sctr
Sh3tc1
Aldh3b2
-Log10 (p-value)
Log2 (fold change)
B
Upregulated genes (Enrichment KEGG)
Thermogenesis
Focal adhesion
Carbon metabolism
AMPK signaling pathway
Insulin signaling pathway
Fatty acid metabolism
Insulin resistance
HIF−1 signaling pathway
PPAR signaling pathway
Central carbon metabolism in cancer
GeneRatio
Count
p.adjust
C
Downregulated genes (Enrichment KEGG)
Coronavirus disease − COVID−19
Ribosome
RNA transport
Endocytosis
Autophagy − animal
Spliceosome
Protein processing in endoplasmic reticulum
Ribosome biogenesis in eukaryotes
Mitophagy − animal
Circadian rhythm
GeneRatio
Count
p.adjust
D
Gene Set Enrichment analysis (GSEA)
TCA cyle
Fatty acid degradation
Glycolysis
Oxidative phosphorylation
Insuling signaling
mTOR signaling
Basal transcription factors
Ribosome biogenesis
MES
E
FLAG-YY1
FLAG-YY1 (S120A)
(kDa)
anti-pAMPK (Thr172)
anti-AMPK
anti-pMTOR (Ser2448)
anti-MTOR
anti-p-p70S6K (Thr389)
anti-p70S6K
anti-TUBULIN

Figure 3

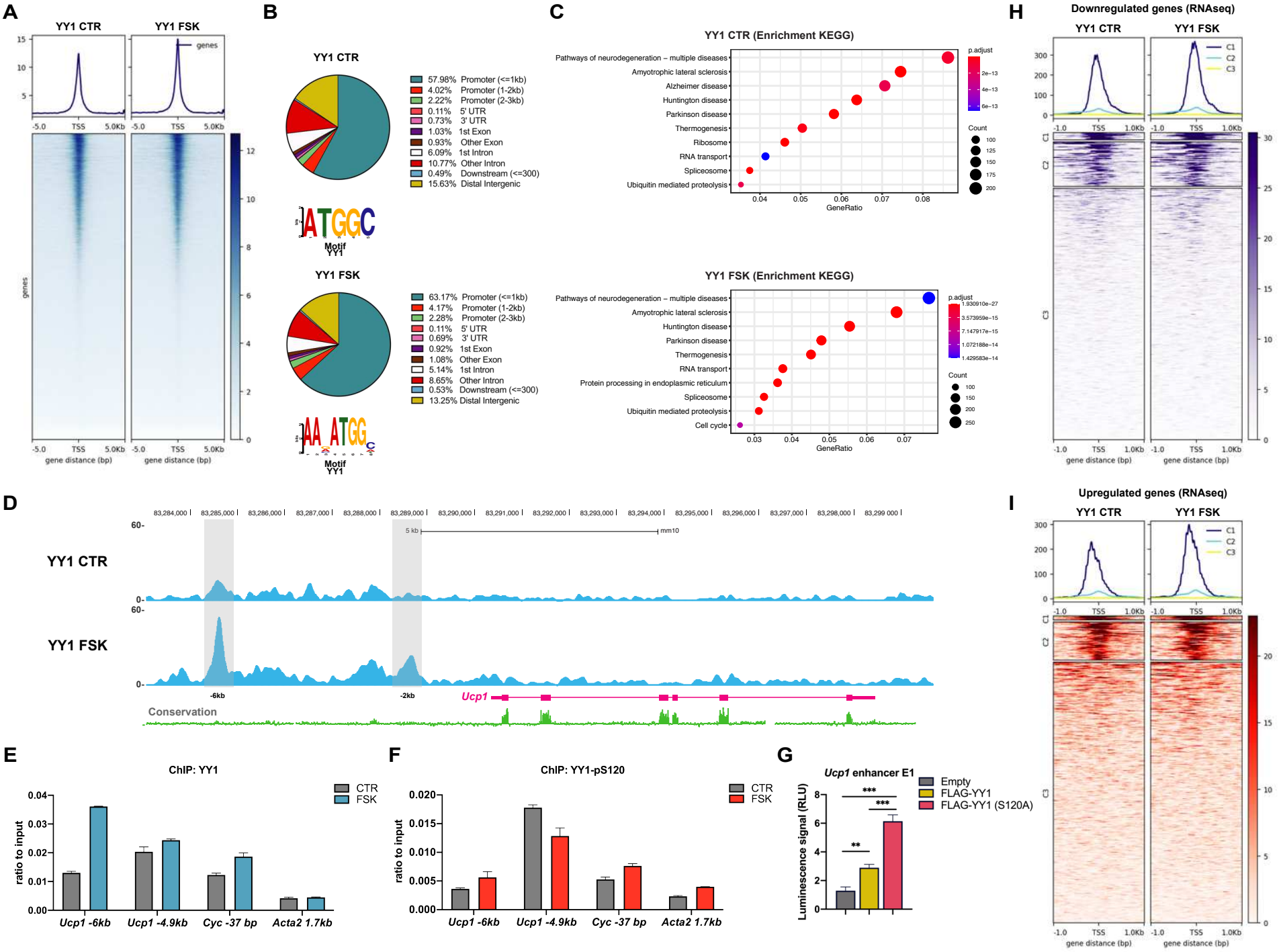
A
YY1 CTR
YY1 FSK
genes
-5.0 TSS 5.0Kb
gene distance (bp)
B
YY1 CTR
57.98% Promoter (<=1kb)
4.02% Promoter (1-2kb)
2.22% Promoter (2-3kb)
0.11% 5' UTR
0.73% 3' UTR
1.03% 1st Exon
0.93% Other Exon
6.09% 1st Intron
10.77% Other Intron
0.49% Downstream (<=300)
15.63% Distal Intergenic
Motif YY1
YY1 FSK
63.17% Promoter (<=1kb)
4.17% Promoter (1-2kb)
2.28% Promoter (2-3kb)
0.11% 5' UTR
0.69% 3' UTR
0.92% 1st Exon
1.08% Other Exon
5.14% 1st Intron
8.65% Other Intron
0.53% Downstream (<=300)
13.25% Distal Intergenic
Motif YY1
C
YY1 CTR (Enrichment KEGG)
Pathways of neurodegeneration – multiple diseases
Amyotrophic lateral sclerosis
Alzheimer disease
Huntington disease
Parkinson disease
Thermogenesis
Ribosome
RNA transport
Spliceosome
Ubiquitin mediated proteolysis
GeneRatio
p.adjust
Count
YY1 FSK (Enrichment KEGG)
Pathways of neurodegeneration – multiple diseases
Amyotrophic lateral sclerosis
Huntington disease
Parkinson disease
Thermogenesis
RNA transport
Protein processing in endoplasmic reticulum
Spliceosome
Ubiquitin mediated proteolysis
Cell cycle
GeneRatio
p.adjust
Count
H
Downregulated genes (RNAseq)
YY1 CTR
YY1 FSK
C1
C2
C3
-1.0 TSS 1.0Kb
gene distance (bp)
D
YY1 CTR
YY1 FSK
5 kb
mm10
-6kb
-2kb
Ucp1
Conservation
I
Upregulated genes (RNAseq)
YY1 CTR
YY1 FSK
C1
C2
C3
-1.0 TSS 1.0Kb
gene distance (bp)
E
ChIP: YY1
CTR
FSK
ratio to input
Ucp1 -6kb
Ucp1 -4.9kb
Cyc -37 bp
Acta2 1.7kb
F
ChIP: YY1-pS120
CTR
FSK
ratio to input
Ucp1 -6kb
Ucp1 -4.9kb
Cyc -37 bp
Acta2 1.7kb
G
Ucp1 enhancer E1
Empty
FLAG-YY1
FLAG-YY1 (S120A)
Luminescence signal (RLU)
**
***
***

Figure 4

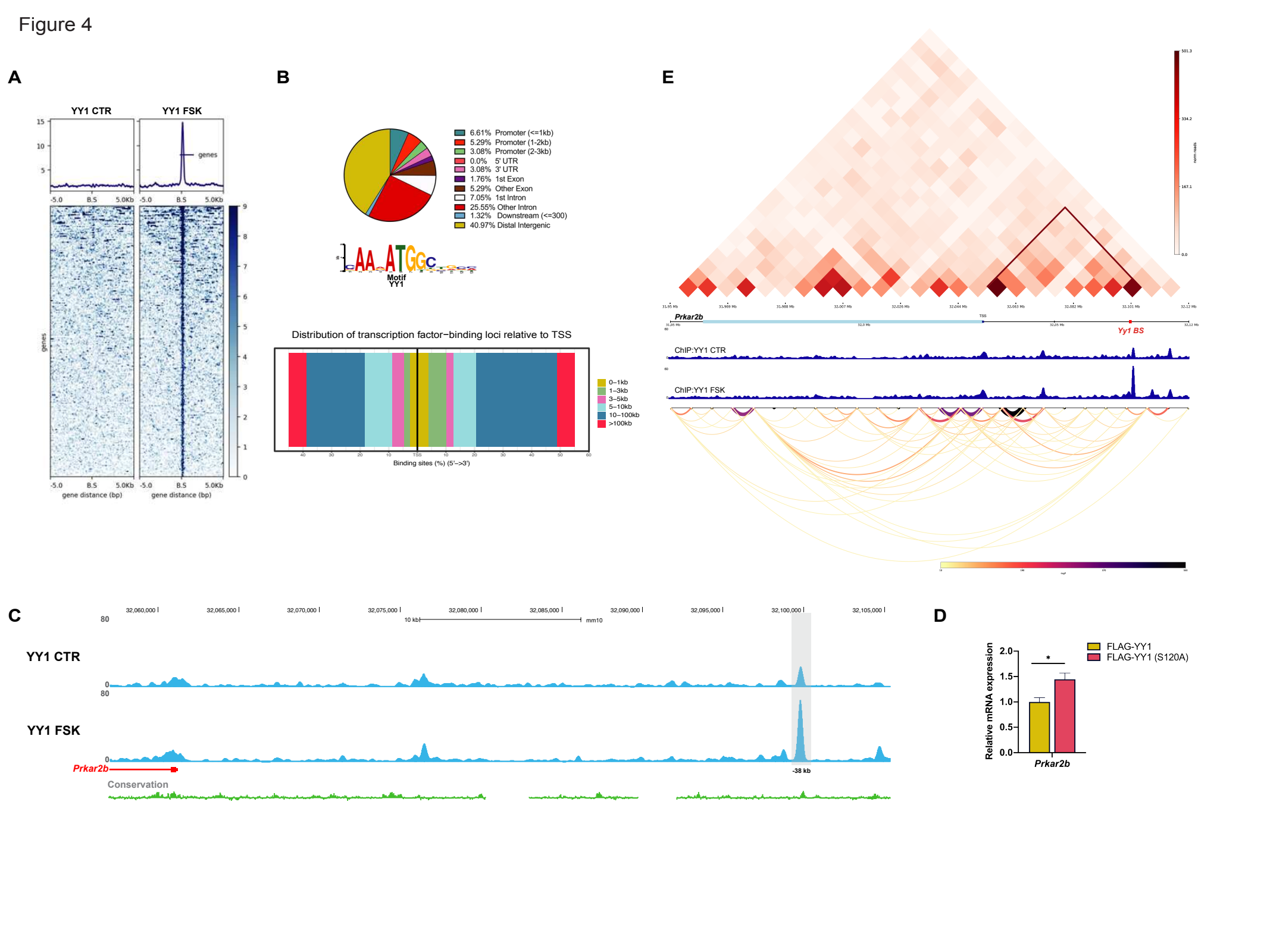
A
YY1 CTR
YY1 FSK
genes
-5.0
B.S
5.0Kb
gene distance (bp)
B
6.61% Promoter (<=1kb)
5.29% Promoter (1-2kb)
3.08% Promoter (2-3kb)
0.0% 5' UTR
3.08% 3' UTR
1.76% 1st Exon
5.29% Other Exon
7.05% 1st Intron
25.55% Other Intron
1.32% Downstream (<=300)
40.97% Distal Intergenic
Motif
YY1
Distribution of transcription factor-binding loci relative to TSS
0–1kb
1–3kb
3–5kb
5–10kb
10–100kb
>100kb
TSS
Binding sites (%) (5'–>3')
E
Prkar2b
Yy1 BS
ChIP:YY1 CTR
ChIP:YY1 FSK
C
10 kb
mm10
YY1 CTR
YY1 FSK
Prkar2b
-38 kb
Conservation
D
Relative mRNA expression
FLAG-YY1
FLAG-YY1 (S120A)
*
Prkar2b

Figure 5

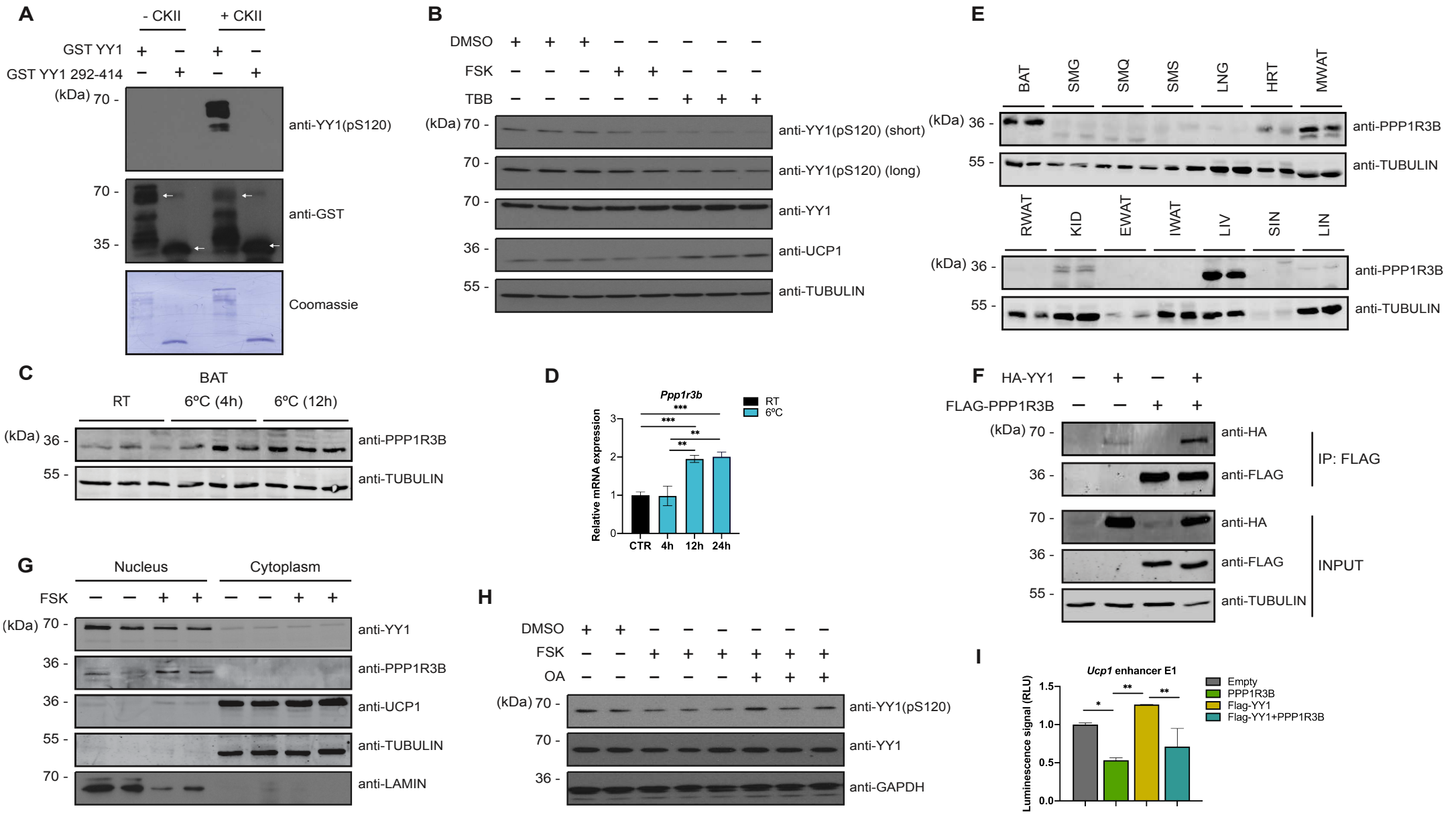
A
- CKII
+ CKII
GST YY1
GST YY1 292-414
(kDa)
70 -
anti-YY1(pS120)
70 -
35 -
anti-GST
Coomassie
B
DMSO
FSK
TBB
(kDa) 70 -
anti-YY1(pS120) (short)
70 -
anti-YY1(pS120) (long)
70 -
anti-YY1
36 -
anti-UCP1
55 -
anti-TUBULIN
E
BAT
SMG
SMQ
SMS
LNG
HRT
MWAT
(kDa) 36 -
anti-PPP1R3B
55 -
anti-TUBULIN
RWAT
KID
EWAT
IWAT
LIV
SIN
LIN
(kDa) 36 -
anti-PPP1R3B
55 -
anti-TUBULIN
C
BAT
RT
6ºC (4h)
6ºC (12h)
(kDa) 36 -
anti-PPP1R3B
55 -
anti-TUBULIN
D
Ppp1r3b
RT
6ºC
Relative mRNA expression
***
***
**
**
CTR
4h
12h
24h
F
HA-YY1
FLAG-PPP1R3B
(kDa) 70 -
anti-HA
36 -
anti-FLAG
IP: FLAG
70 -
anti-HA
36 -
anti-FLAG
55 -
anti-TUBULIN
INPUT
G
Nucleus
Cytoplasm
FSK
(kDa) 70 -
anti-YY1
36 -
anti-PPP1R3B
36 -
anti-UCP1
55 -
anti-TUBULIN
70 -
anti-LAMIN
H
DMSO
FSK
OA
(kDa) 70 -
anti-YY1(pS120)
70 -
anti-YY1
36 -
anti-GAPDH
I
Ucp1 enhancer E1
Luminescence signal (RLU)
Empty
PPP1R3B
Flag-YY1
Flag-YY1+PPP1R3B
*
**
**

Figure 6

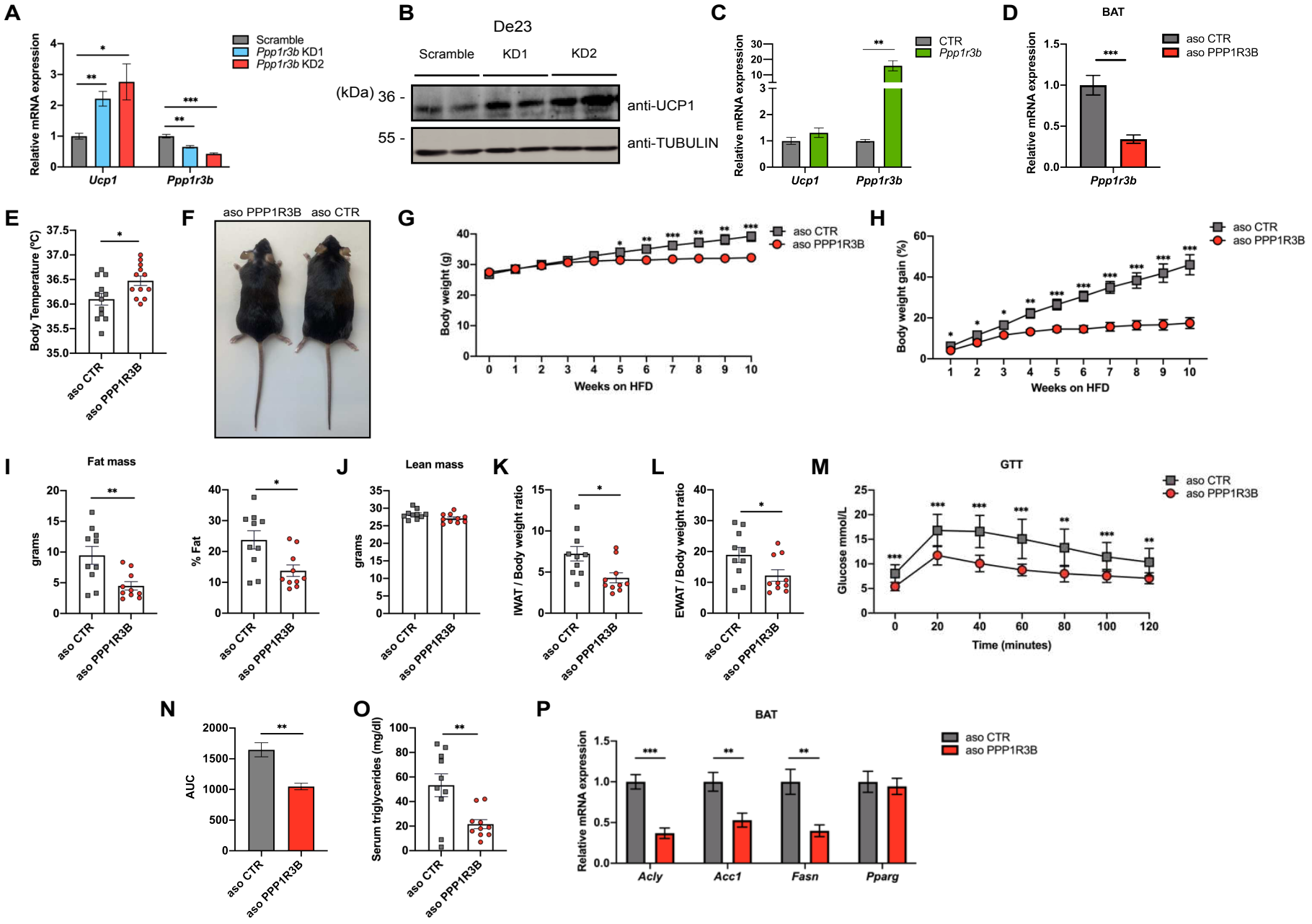
A
Relative mRNA expression
Scramble
Ppp1r3b KD1
Ppp1r3b KD2
Ucp1
Ppp1r3b
B
De23
Scramble
KD1
KD2
(kDa)
36 -
55 -
anti-UCP1
anti-TUBULIN
C
Relative mRNA expression
CTR
Ppp1r3b
Ucp1
Ppp1r3b
D
BAT
Relative mRNA expression
aso CTR
aso PPP1R3B
Ppp1r3b
E
Body Temperature (ºC)
aso CTR
aso PPP1R3B
F
aso PPP1R3B
aso CTR
G
Body weight (g)
aso CTR
aso PPP1R3B
Weeks on HFD
H
Body weight gain (%)
aso CTR
aso PPP1R3B
Weeks on HFD
I
Fat mass
grams
% Fat
aso CTR
aso PPP1R3B
J
Lean mass
grams
K
IWAT / Body weight ratio
L
EWAT / Body weight ratio
M
GTT
Glucose mmol/L
Time (minutes)
aso CTR
aso PPP1R3B
N
AUC
O
Serum triglycerides (mg/dl)
P
BAT
Relative mRNA expression
Acly
Acc1
Fasn
Pparg
aso CTR
aso PPP1R3B

Supplementary Figure 1

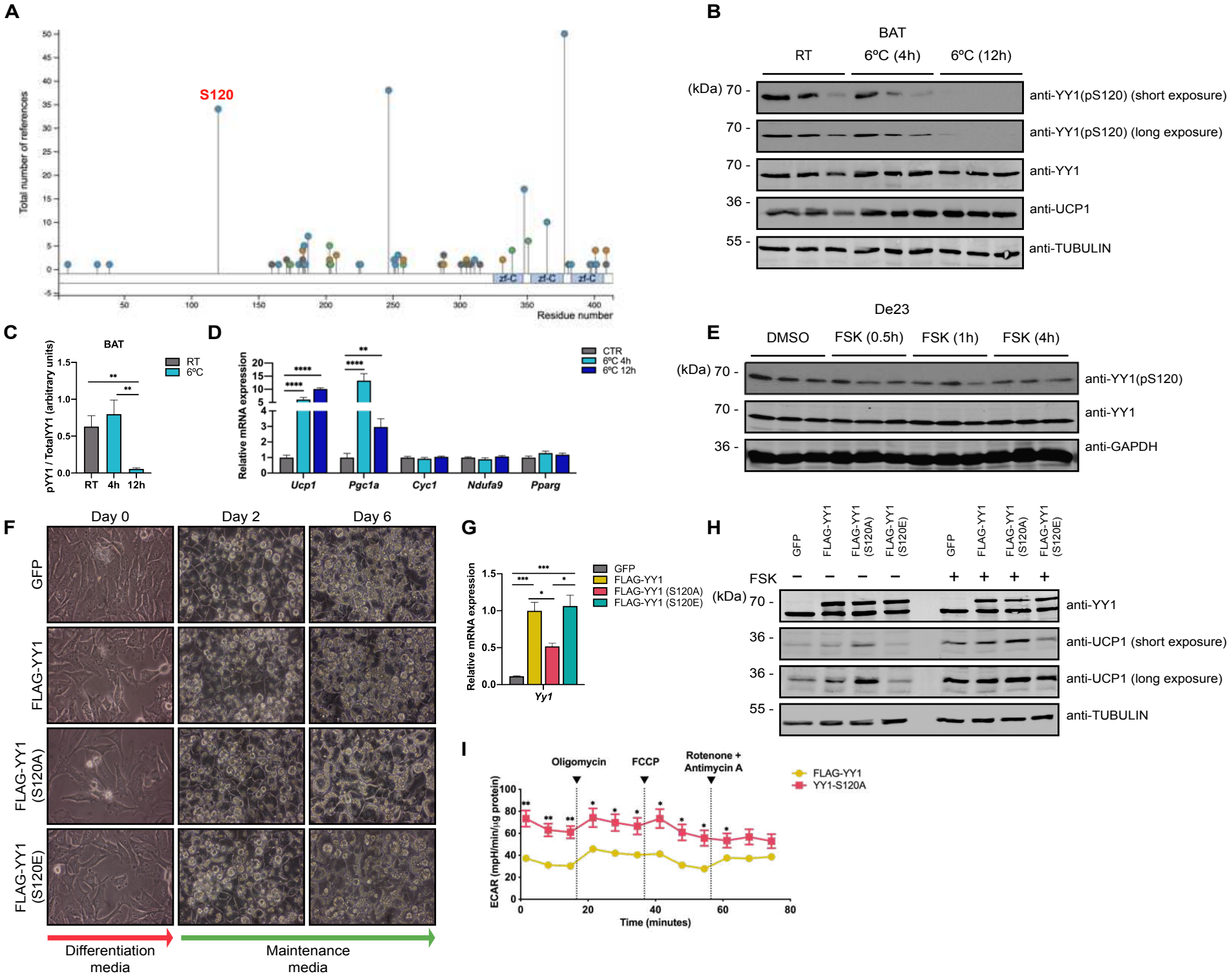

Supplementary Figure 2

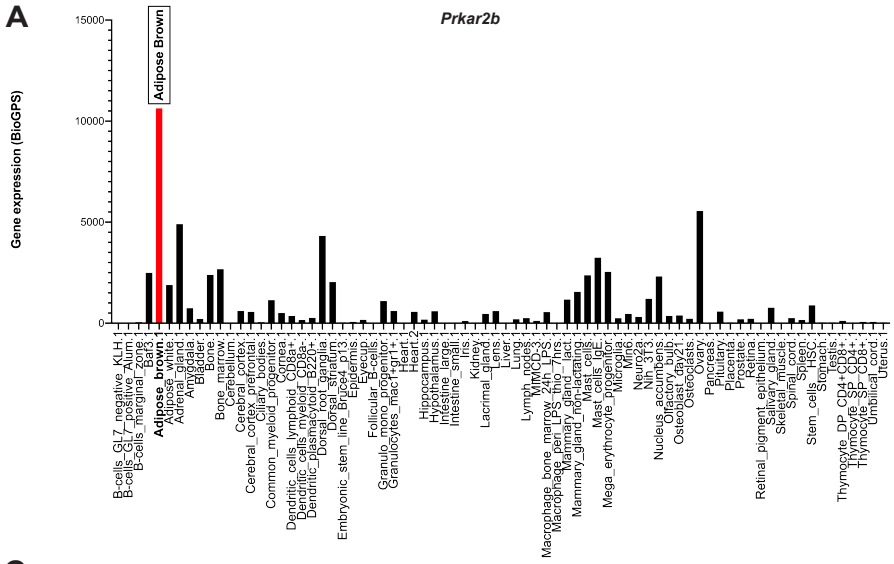

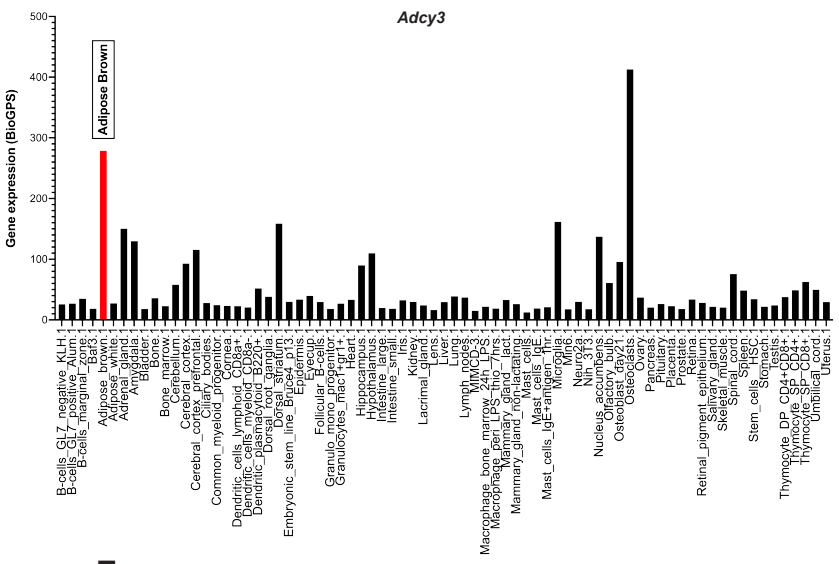

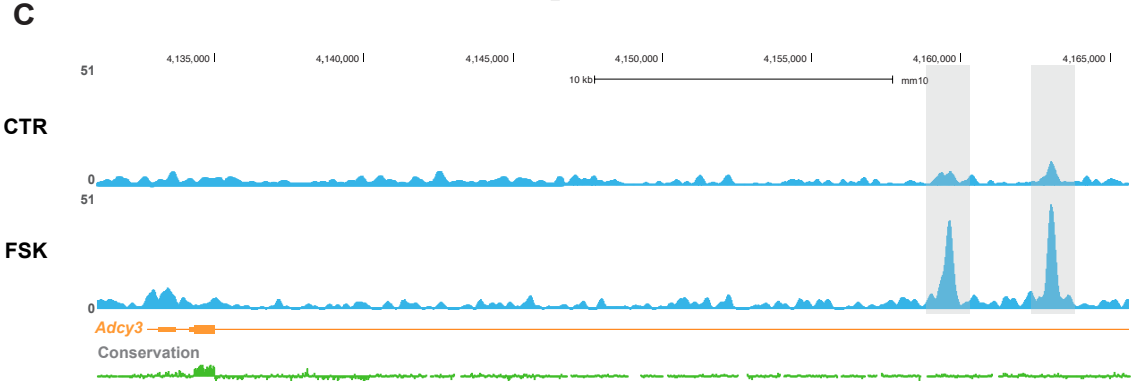

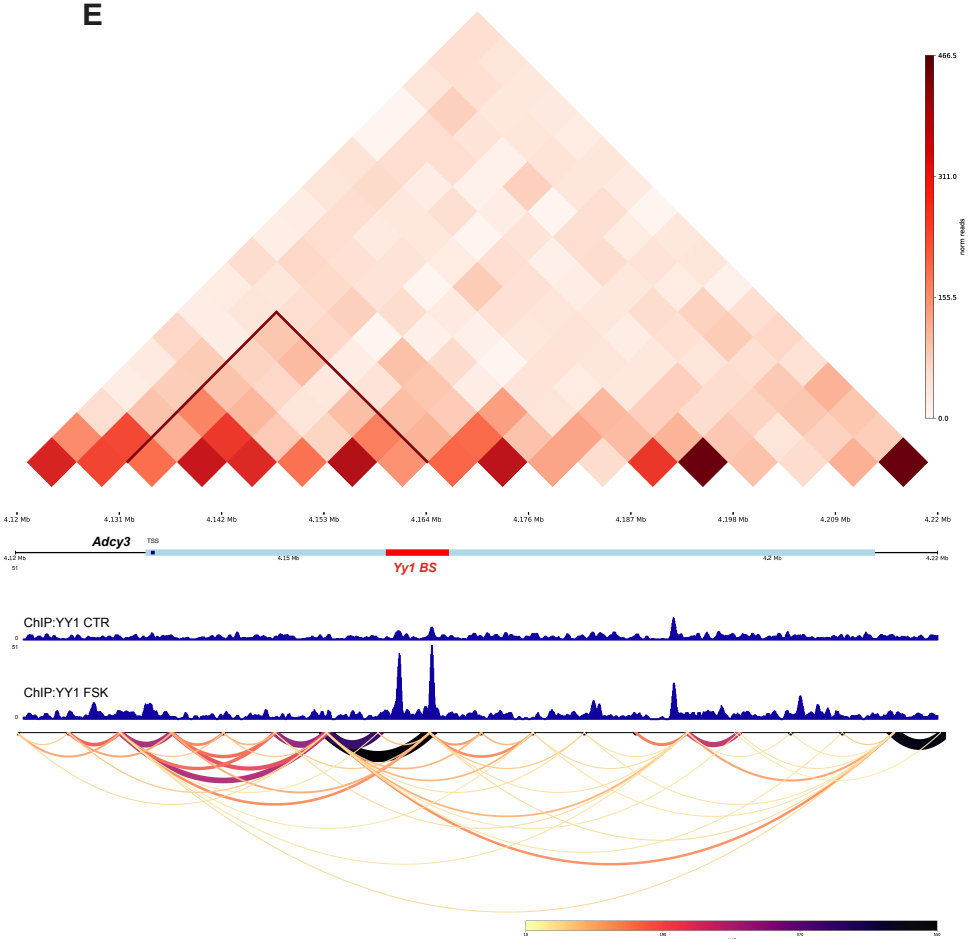

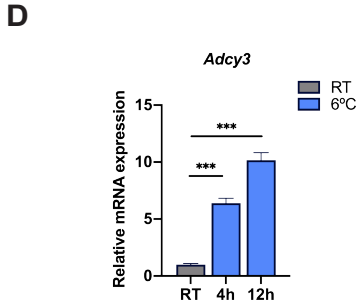

Supplementary Figure 3

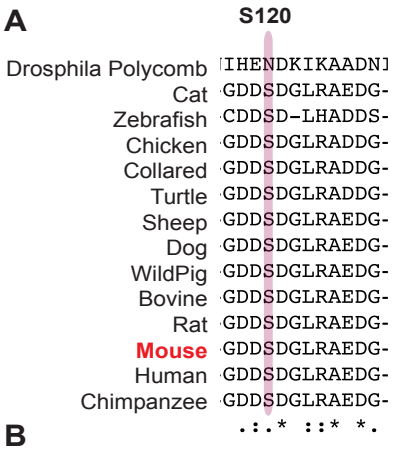

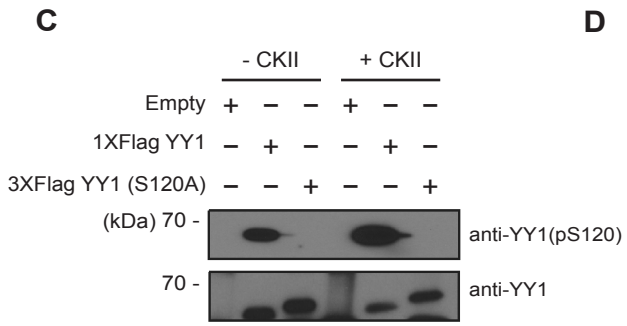

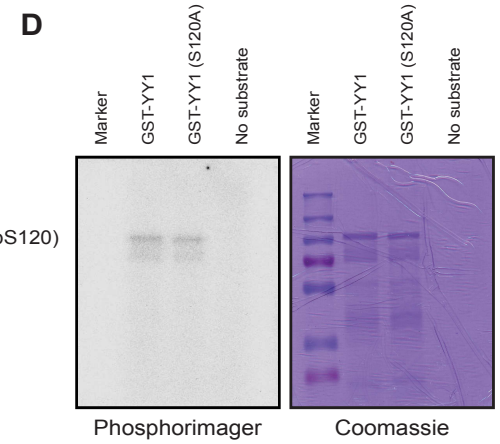

B

Gene symbol	motif name	motif group	score	percentile	protein	site	site sequence
PRKACG	Protein Kinase A	Basophilic serine/threonine kinasegroup	0.3424	0.002360114	TYY1_MOUSE	S365	EGCGKRFsLDFNLRT
AURKA	Aurora A	Basophilic serine/threonine kinasegroup	0.4207	0.001800772	TYY1_MOUSE	S365	EGCGKRFsLDFNLRT
PRKCD	PKC delta	Basophilic serine/threonine kinasegroup	0.4542	0.021449199	TYY1_MOUSE	S184	GKKSGKKsYLGGGAG
PRKCA	PKC alpha/beta/gamma	Basophilic serine/threonine kinasegroup	0.4703	0.013952431	TYY1_MOUSE	S180	KKGGGKKsGKKSYLG
PRKCE	PKC epsilon	Basophilic serine/threonine kinasegroup	0.4993	0.037484059	TYY1_MOUSE	S184	GKKSGKKsYLGGGAG
PRKCZ	PKC zeta	Basophilic serine/threonine kinasegroup	0.5092	0.017087279	TYY1_MOUSE	S311	TKMFRDNsAMRKHLH
AURKB	Aurora B	Basophilic serine/threonine kinasegroup	0.525	0.006144072	TYY1_MOUSE	S365	EGCGKRFsLDFNLRT
PRKCZ	PKC zeta	Basophilic serine/threonine kinasegroup	0.5373	0.026795272	TYY1_MOUSE	S180	KKGGGKKsGKKSYLG
NEK1	Nek1	Phosphoserine/threonine binding group	0.5574	0.003443866	TYY1_MOUSE	S397	CNKKFAQsTNLKSHI
MAPK3	Erk1 Kinase	Proline-dependent serine/threoninekinase group	0.568	0.017353519	TYY1_MOUSE	S247	EQIIGENsPPDYSEY
CAMK2G	Calmodulin dependent Kinase 2	Basophilic serine/threonine kinasegroup	0.5828	0.040857212	TYY1_MOUSE	S220	KTLEGEFsVTMWSSD
CSNK2B	**Casein Kinase 2**	**Acidophilic serine/threonine kinase group**	**0.5893**	**0.04805193**	**TYY1_MOUSE**	**S120**	**EVVGGDDsDGLRAED**
CAMK2G	Calmodulin dependent Kinase 2	Basophilic serine/threonine kinasegroup	0.5936	0.048724448	TYY1_MOUSE	S365	EGCGKRFsLDFNLRT
PRKACG	Protein Kinase A	Basophilic serine/threonine kinasegroup	0.5987	0.042990609	TYY1_MOUSE	S184	GKKSGKKsYLGGGAG
CDK5	Cdk5 Kinase	Proline-dependent serine/threoninekinase group	0.6379	0.049152623	TYY1_MOUSE	S247	EQIIGENsPPDYSEY
NEK4	Nek4	Phosphoserine/threonine binding group	0.6823	0.015201481	TYY1_MOUSE	S397	CNKKFAQsTNLKSHI
NEK2	Nek2	Phosphoserine/threonine binding group	0.7088	0.027945404	TYY1_MOUSE	S397	CNKKFAQsTNLKSHI
NEK1	Nek1	Phosphoserine/threonine binding group	0.7138	0.027740805	TYY1_MOUSE	S337	CGKAFVEsSKLKRHQ
NEK9	Nek9	Phosphoserine/threonine binding group	0.7437	0.020648244	TYY1_MOUSE	S167	KSGGGASsGGGRVKK
NEK1	Nek1	Phosphoserine/threonine binding group	0.7545	0.042944729	TYY1_MOUSE	S220	KTLEGEFsVTMWSSD
NEK10	Nek10 S	Phosphoserine/threonine binding group	0.7638	0.02149723	TYY1_MOUSE	S167	KSGGGASsGGGRVKK
NEK5	Nek5	Phosphoserine/threonine binding group	0.7681	0.033011884	TYY1_MOUSE	S311	TKMFRDNsAMRKHLH
NEK6	Nek6	Phosphoserine/threonine binding group	0.7821	0.022833944	TYY1_MOUSE	S166	GKSGGGAsSGGGRVK
NEK4	Nek4	Phosphoserine/threonine binding group	0.7928	0.043391386	TYY1_MOUSE	S337	CGKAFVEsSKLKRHQ
NEK3	Nek3	Phosphoserine/threonine binding group	0.7986	0.030313811	TYY1_MOUSE	S220	KTLEGEFsVTMWSSD
NEK7	Nek7	Phosphoserine/threonine binding group	0.7988	0.030452779	TYY1_MOUSE	S220	KTLEGEFsVTMWSSD
NEK6	Nek6	Phosphoserine/threonine binding group	0.8173	0.032975707	TYY1_MOUSE	S167	KSGGGASsGGGRVKK
NEK7	Nek7	Phosphoserine/threonine binding group	0.8231	0.038381118	TYY1_MOUSE	S397	CNKKFAQsTNLKSHI
NEK10	Nek10 S	Phosphoserine/threonine binding group	0.8253	0.044663944	TYY1_MOUSE	S166	GKSGGGAsSGGGRVK
NEK3	Nek3	Phosphoserine/threonine binding group	0.8434	0.045430614	TYY1_MOUSE	S397	CNKKFAQsTNLKSHI

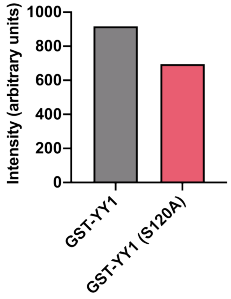

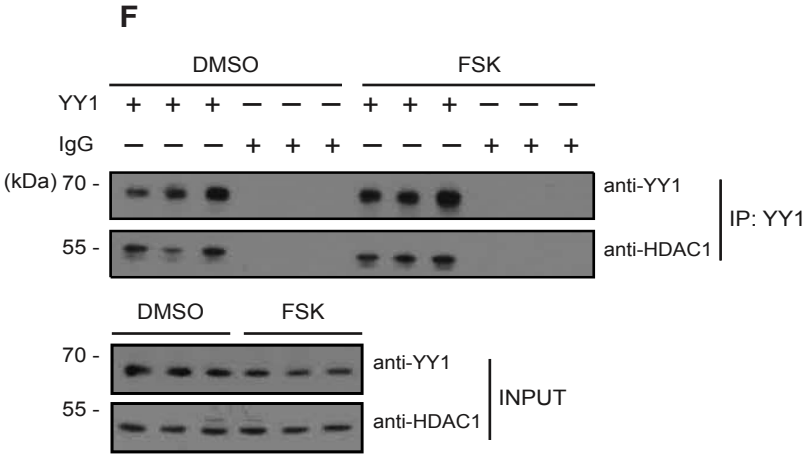

Supplementary Figure 4

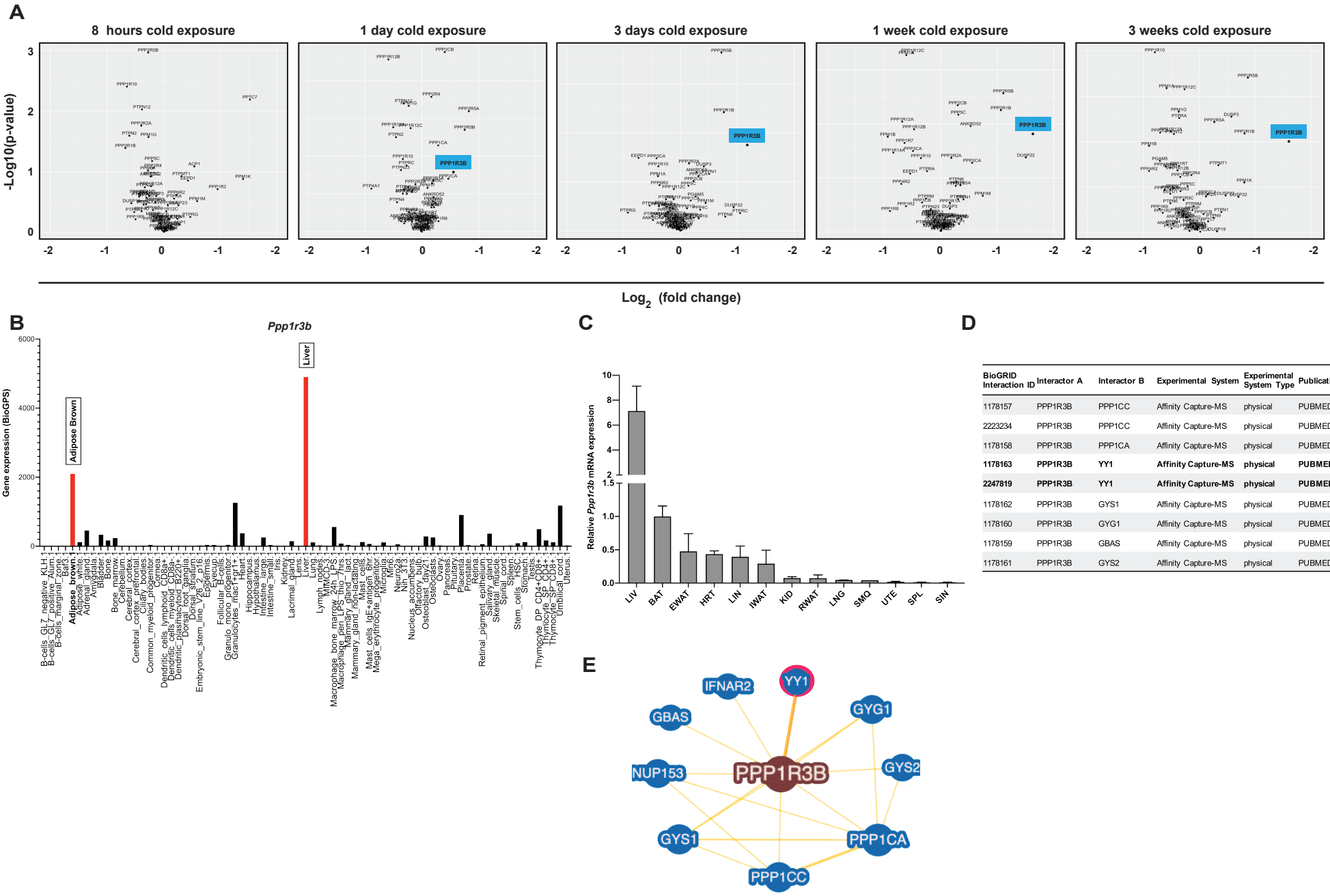

D

BioGRID Interaction ID	Interactor A	Interactor B	Experimental System	Experimental System Type	Publication Source	Score	SWISS-PROT Accessions Interactor B
1178157	PPP1R3B	PPP1CC	Affinity Capture-MS	physical	PUBMED:26186194	0.99999737	P36873
2223234	PPP1R3B	PPP1CC	Affinity Capture-MS	physical	PUBMED:28514442	0.99998848	P36873
1178158	PPP1R3B	PPP1CA	Affinity Capture-MS	physical	PUBMED:26186194	0.99228221	P62136
1178163	**PPP1R3B**	**YY1**	**Affinity Capture-MS**	**physical**	**PUBMED:26186194**	**0.97685973**	**P25490**
2247819	**PPP1R3B**	**YY1**	**Affinity Capture-MS**	**physical**	**PUBMED:28514442**	**0.96953517**	**P25490**
1178162	PPP1R3B	GYS1	Affinity Capture-MS	physical	PUBMED:26186194	0.95524605	P13807
1178160	PPP1R3B	GYG1	Affinity Capture-MS	physical	PUBMED:26186194	0.9038814	P46976
1178159	PPP1R3B	GBAS	Affinity Capture-MS	physical	PUBMED:26186194	0.86096442	O75323
1178161	PPP1R3B	GYS2	Affinity Capture-MS	physical	PUBMED:26186194	0.78777723	P54840

Supplementary Figure 5

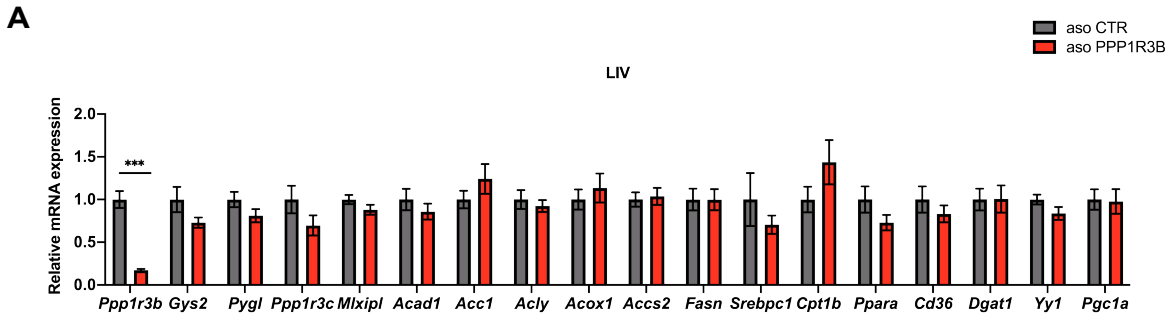

SUPPLEMENTARY FIGURE LEGENDS.

Figure S1. YY1-S120 dephosphorylation in brown adipocytes induces thermogenesis.

A) Known phosphorylation sites within YY1 mouse protein, image obtained from PhosphoSitePlus® . **B)** WB analysis of BAT isolated from mice at room temperature (RT) (25°C) or exposed to cold (6 °C) for 4 and 12 hours and **C)** Quantification of band intensities, performed using ImageJ**. D)** Relative mRNA analysis of BAT isolated from mice at room temperature (RT) (25°C) or exposed to cold (6 °C) for 4 and 12 hours. **E)** Time course of YY1-S120 dephosphorylation in response to FSK (10 µM) versus DMSO control in differentiated De23 brown adipocyte cell line. **F)** Representative micrographs of mutant adipocytes cell lines during the differentiation process. **G)** Relative mRNA expression versus endogenous reference gene *Rpl13*. **H)** WB from differentiated brown adipocytes treated with FSK (10 µM) for 4h versus DMSO control in mutant YY1 cell lines. WB detection was performed using specific antibodies for YY1, UCP1 and Tubulin or GAPDH as a loading control. **I)** Extra cellular acidification rate (ECAR) measured at the basal level followed by the addition of oligomycin (5 µM), FCCP (1 µM), and antimycin A and rotenone (5 µM) using a Seahorse Analyzer. Error bars indicate SEM. Statistically significant differences shown by Student t-test *** p-value <0.001,** p-value <0.01 and * p-value <0.05.

Figure S2. Dephosphorylated YY1-S120 binds to *Adcy3* locus.

A, B) *Prkar2b* and *Adcy3* gene expression across different mouse tissues. Data, in arbitrary expression units, obtained from the BioGPS database. Adipose brown tissue (red bar). **C)** Genome browser ChIP-seq tracks of YY1 binging at the *Adcy3* locus. **D)** *Adcy3* expression in BAT isolated from mice at room temperature (RT) (22°C) or exposed to cold (6 °C) for 4 and 12 hours. **E)** *Adcy3* locus showing Hi-C matrix and YY1 ChIPseq track. Error bars indicate

SEM. Statistically significant differences shown by Student t-test *** p-value <0.001,** p-value <0.01 and * p-value <0.05.

Figure S3. CK2 phosphorylates YY1 at S120 in brown adipocytes.

A) Alignment of YY1 protein sequence across species. **B)** Scansite predicted kinase motifs for YY1**. C)** In vitro cold kinase assay of purified Flag-YY1 from transfected brown adipocytes and recombinant CK2, followed by detection with YY1-(pS120) specific antibody. **D)** Radioactive kinase assay. GST-tagged YY1-WT and phospho mutant YY1-S120A were used in the radioactive in vitro kinase reaction. No-substrate kinase reaction served as a negative control. Recombinant CKII was added to the kinase assay mix and separated on 10% SDS-PAGE gels for Coomassie staining and read on a phosphorimager screen (1 h incubation). **E)** Quantification of band intensities from radioactive kinase assay represented blot was performed using ImageJ. **F)** YY1 immunoprecipitation in U2OS transfected cells and detection of interaction with HDAC1 antibodies in cells treated with FSK.

Figure S4. Identification of PPP1R3B as a cold-induced factor in brown adipose tissue.

A) Volcano plots of all protein phosphatases and associated regulatory subunits identified by mass-spectrometry in brown adipose tissue of mice exposed to cold for 8 hours, 1 day, 3 days 1 week and 3 weeks normalized to thermoneutrality conditions. Data obtained from Sustarsic et al., 2018 proteomic dataset. **B)** *Ppp1r3b* gene expression across different mouse tissues. Data, in arbitrary expression units, obtained from the BioGPS database. Liver and BAT are shown in red bars. **C)** Relative mRNA analysis of *Ppp1r3b* expression in different mouse tissues versus endogenous reference gene *Rpl13.* **D)** Table showing the experimentally verified protein-protein interactions from the BioGRID database. **E)** Network showing the experimentally verified protein-protein interactions from the BioGRID database.

Figure S5. *Ppp1r3b* knockdown and liver gene expression.

A) Relative mRNA expression in liver of aso CTR and aso PPP1R3B HFD mice**.** Data represented means of 10 mice per group. Error bars indicate SEM. Statistically significant differences shown by Student t-test *** p-value <0.001,** p-value <0.01 and * p-value <0.05.